University of Pardubice

Faculty of Economics and Administration

Institute of Systems Engineering and Informatics

ASSESSING VEGETATION CHANGE USING SATELLITE IMAGERY ANALYSIS

Master Thesis

2025

Univerzita Pardubice
Fakulta ekonomicko-správní
Akademický rok: 2023/2024

ZADÁNÍ DIPLOMOVÉ PRÁCE

(projektu, uměleckého díla, uměleckého výkonu)

Jméno a příjmení:	**Emmanuel Amponsem**
Osobní číslo:	**E23963**
Studijní program:	**N0688A140008 Informatics and System Engineering**
Specializace:	**Informatics in Public Administration**
Téma práce:	**Assessing Vegetation using Satellite Imagery Analysis**
Zadávající katedra:	**Ústav systémového inženýrství a informatiky**

Zásady pro vypracování

The aim of this thesis is to compare selected methods of satellite vegetation delineation or change detection and use the chosen method to assess vegetation change in recent years in a selected area of interest. This work will emphasize the importance of accurate and reliable vegetation monitoring for environmental management.

Outline:

Vegetation Change Detection Methods.
Proposal of a Procedure for Vegetation Change Detection.
Analysis and Interpretation of Findings.
Conclusion and Recommendations

Rozsah pracovní zprávy: **approx. 50 pages**
Rozsah grafických prací:
Forma zpracování diplomové práce: **tištěná/elektronická**
Jazyk zpracování: **Angličtina**

Seznam doporučené literatury:

AFIFY, H. A., 2011. Evaluation of change detection techniques for monitoring land-cover changes: A case study in New Burg El-Arab area. *Alexandria Engineering Journal, 50*(2), pp. 187-195. https://doi.org/10.1016/j.aej.2011.06.001
CAMPBELL, James B. and WYNNE, Randolph H., 2011. *Introduction to Remote Sensing, Fifth Edition*. Guilford Press. ISBN 978-1-60918-177-2.
EMILIO CHUVIECO, 2016. *Fundamentals of Satellite Remote Sensing – An Environmental Approach*. Second Edition. Boca Raton, FL: Taylor & Francis Group. ISBN 978-1-4987-2807-2.
WULDER, Michael A. and FRANKLIN, Steven E., 2012. *Remote Sensing of Forest Environments: Concepts and Case Studies*. Springer Science & Business Media. ISBN 978-1-4615-0306-4.

Vedoucí diplomové práce: **Ing. Tomáš Brunclík, Ph.D.**
Ústav systémového inženýrství a informatiky

Datum zadání diplomové práce: **1 září 2024**
Termín odevzdání diplomové práce: **30. Dubna 2025**

L.S

prof. Ing. Jan Stejskal, Ph.D. v.r.
děkan

prof. Ing. Jitka komárková, Ph.D. v.r.
garant studijního program

V Pardubicích dne 1. září 2024

AUTHOR'S STATEMENT

I declare:

I developed the work entitled **ASSESSING VEGETATION CHANGE USING SATELLITE IMAGERY ANALYSIS** on my own. All literary sources and information that I used in my work are listed in the list of used literature.

I have been made aware that my work is subject to the rights and obligations arising from Act No. 121/2000 Coll., on copyright, on rights related to copyright and on the amendment of certain laws (the Copyright Act), as amended, in particular the fact that the University of Pardubice has the right to conclude a license agreement for the use of this work as a school work according to § 60, paragraph 1 of the Copyright Act, and that if the use of this work by me or a license to use it will be granted to another subject, the University of Pardubice is entitled to demand from me a reasonable contribution to cover the costs incurred to create the work, up to their actual amount, depending on the circumstances.

I acknowledge that in accordance with § 47b of Act No. 111/1998 Coll., on universities and on the amendment and addition of other laws (the Act on Universities), as amended, and the University of Pardubice Directive No. 7/2019 Rules for submission, publication and formal editing of final theses, as amended, the thesis will be published through the Digital Library of the University of Pardubice.

In Pardubice, 30.04.2025 Emmanuel Amponsem, b.o.h.

ACKNOWLEDGEMENT

First and foremost, I express my heartfelt gratitude to God Almighty, whose grace, strength, and guidance have sustained me throughout this academic journey. Without His favor, completing this research thesis would not have been possible.

I would like to extend my sincere appreciation to my supervisor, Ing. Tomáš Brunclík, Ph.D., for his patience, guidance, and constructive feedback throughout the entire research process. His professional insight and support helped shape this work, and I am grateful for the opportunity to learn under his mentorship.

I am deeply thankful to my family for your unwavering love, encouragement, and prayers. Your belief in me has been my source of strength through this journey's challenging and rewarding moments. I owe special thanks to my parents, whose sacrifices and constant support have laid the foundation for all my academic and personal achievements.

I am also grateful to the faculty members, lecturers, and professors who contributed to my growth during my study time. Their dedication to teaching and mentorship has played a critical role in shaping my academic foundation.

Lastly, I acknowledge the vital role of Google Earth Engine (GEE), whose powerful cloud-based platform enabled this study's core analysis and visualization. Its accessibility and tools greatly enhanced the scope and depth of this research.

This research is lovingly dedicated to Nana Akwasi Amponsem Acheampong, Bernice Acheampong, and Comfort Amoah, who have been my backbone throughout life. His encouragement, belief in my potential, and unwavering support were instrumental in my decision to pursue a master’s degree. Thank you for being my most significant source of strength and inspiration.

ANNOTATION

This study analyzed vegetation changes in the Miombo woodlands of Central Zambia using Sentinel-2 satellite imagery and vegetation indices—NDVI and EVI—across two time periods: 2017–2018 and 2022–2023. The objective was to assess spatial vegetation dynamics, classify vegetation cover, and evaluate classification accuracy through both threshold-based and supervised machine learning approaches. Ground truth samples were manually collected and utilized for validation. Results revealed significant shifts in vegetation classes over time, with Random Forest classification providing improved accuracy over threshold-based methods. The findings highlight the utility of remote sensing techniques combined with Google Earth Engine for monitoring vegetation trends in Miombo ecosystems, offering valuable insights for sustainable land use planning and ecological assessment in Central Zambia.

KEYWORDS

Central Zambia, Miombo woodland, NDVI, EVI, vegetation classification, Sentinel-2, Google Earth Engine, Random Forest, land cover change, remote sensing.

ANOTACE

Tato studie analyzuje změny vegetace v lesích Miombo ve střední Zambii pomocí satelitních snímků Sentinel-2 a vegetačních indexů NDVI a EVI během dvou časových období: 2017–2018 a 2022–2023. Cílem bylo posoudit prostorovou dynamiku vegetace, klasifikovat vegetační pokryv a vyhodnotit přesnost klasifikace pomocí prahových metod i strojového učení. Byla ručně shromážděna validační data, která sloužila k ověření výsledků. Výsledky odhalily výrazné změny ve vegetačních třídách a ukázaly vyšší přesnost klasifikace metodou Random Forest. Studie poukazuje na efektivitu využití metod dálkového průzkumu Země ve spojení s Google Earth Engine pro sledování vegetačních trendů v ekosystémech Miombo a nabízí cenné poznatky pro udržitelné plánování využívání půdy ve střední Zambii.

KLÍČOVÁ SLOVA

Střední Zambie, Miombo, NDVI, EVI, klasifikace vegetace, Sentinel-2, Google Earth Engine, Random Forest, změna vegetačního pokryvu, dálkový průzkum Země

CONTENTS

LIST OF TABLES

LIST OF FIGURES

LIST OF GRAPHS

LIST OF ABBREVIATIONS

INTRODUCTION

Miombo woodlands represent one of Africa's important and large tropical dry forest ecosystems, covering about 2.7 million km² across eastern, central, and southern Africa. They are identified by the domination of Brachystegia, Julbernardia, and Isoberlina tree species and form a critical ecological transformation zone between the tropical forests and southern savannas (Frost, 1996). The miombo ecology provides important ecosystem services such as carbon sequestration, water regulation, and conservation of biodiversity while supporting the livelihoods of over 100 million people by providing food, fuel, medicine, and construction materials (Ryan et al., 2016).

Despite their importance ecologically and socioeconomically, Miomobo woodlands face unmatched pressures from human-driven activities and climate change. Deforestation rates in some Miombo regions exceed 2% every year, influenced mainly by the production of charcoal, expansion of agriculture, extraction of timber, and infrastructure development. For instance, between 2003 and 2013, the average annual deforestation rate in Mozambique's Nampula province reached 4.35% (Magalhães, 2025). Similarly, in the Lubumbashi region of the Democratic Republic of Congo, the yearly deforestation from 1990 to 2022 was about 1.51% (Muteya et al., 2023). The fast growth of agriculture in Miombo woodlands has led to cutting down all trees, which leads to the loss of species and important natural benefits like clean water and air (Kalaba et al., 2013). Additionally, studies estimate rainfall in the Miombo region has been reduced by 5 to 15% due to climate change, coupled with more frequent fires posing a serious threat to this ecosystem (Pungulanhe et al., 2021).

Good tracking of vegetation changes over time in the Miombo woodlands is very much needed. Traditional field studies give detailed information but cannot cover larger areas very often. Satellite monitoring offers a better way to monitor vegetation changes across this big ecosystem at scales and times. Studies have shown the use of satellite imagery like PlanetScope in mapping the tree species in Miombo woodlands. This mapping is very important for effective monitoring and management of these forests (Nkya et al., 2024a).

For several decades, satellite remote sensing has completely changed our ability to detect and track changes in the environment over large areas. Satellite imagery like Landsat and Sentinel being freely accessible has allowed researchers to study past changes in land use and nature to fully understand how these changes happened over time and create a starting point to compare

future changes (Wulder et al., 2019). The creation of much more advanced techniques for detecting changes across many different natural settings has been possible due to breakthroughs and the growing power of how computers process images. Scientists can now track environmental shifts with tools that were not possible just a few years back, giving us new eyes on changing landscapes (G. Cheng et al., 2024).

1. RESEARCH FRAMEWORK AND OBJECTIVES

1.1 Research Problem

In 2004, it was stated despite the recognized importance of monitoring vegetation dynamics in Miombo woodlands, there were many uncertainties regarding the most suitable methodologies for detecting using satellite imagery. A large part of earlier approaches relied on simple techniques like image differencing, classification comparisons, basic time series analysis and principal component analysis (Coppin et al., 2004; Lu et al., 2004). The past two decades has seen transformational improvements in technology and analytical methods that have mostly resolved these uncertainties. Modern approaches now leverage artificial intelligence and deep learning frameworks showing significant accuracy improvements over traditional methods (Waldeland et al., 2022). The integration of multiple sensor types, combining optical, radar and LiDAR data has overcome the constant challenge of cloud cover that limited earlier monitoring efforts (Scoles, 2022). Now, new time series approaches can better differentiate between climate changes caused by human activities and those that happen naturally (Zimba et al., 2024), while cloud computing platforms make it possible to analyze entire continents, something that was previously impossible because computers were not powerful enough (Hamunyela et al., 2020).

Studies conducted in the mid and late 2010s documented vegetation changes in specific Miombo regions using remote sensing techniques (Bhattarai et al., 2020; Schneibel et al., 2017), recent reviews have highlighted important progress in developing standard methods for monitoring these critical ecosystems. The past five years have seen strong frameworks that compare and integrate multiple methodologies (Demol et al., 2024; Wu et al., 2022). These frameworks have been highly embraced by conservation practitioners and policymakers tasked with implementing sustainable management strategies and reporting for international commitments such as REDD+ (Reducing Emissions from Deforestation and Forest Degradation) and sustainable development goals (Köhl et al., 2009). Modern approaches now focus attention on participatory monitoring systems that combine satellite based observations with common knowledge (N'tambwe Nghonda et al., 2025).

1.2 Research Aims and Objectives

The primary purpose of this research is to assess vegetation change in Miombo woodlands using advanced satellite imagery analysis techniques that have emerged in recent years. While traditional vegetation indices have been used for decades, this study mainly focuses on comparing the effectiveness of the Enhanced Vegetation Index (EVI) and the Normalized Difference Vegetation Index (NDVI) within the context of modern machine learning classification frameworks and time series analysis methods. This research builds upon recent methodological advances to develop and implement a structured approach for monitoring vegetation dynamics that aligns with current best practices for Miombo ecosystem assessment (Loiola et al., 2023).

The specific objectives include:

- To evaluate and compare how well EVI and NDVI work with modern machine learning methods to classify Miombo woodland areas into four meaningful categories (bare land, grassland, open woodland, and dense woodland) (Kamusoko et al., 2014)
- To test and assess advanced methods for detecting landscape changes, focusing on techniques that continuously monitor changes and break down time patterns in data (Decuyper et al., 2022; Y. Zhang et al., 2022). The study will use satellite images from two time periods, 2017-2018 and 2022-2023, to measure and track how vegetation has changed across the study area.
- To investigate where and how vegetation has changed using modern statistical methods that can recognize spatial patterns (Bhattarai et al., 2020) identifying areas of vegetation loss, gain, and stability while accounting for seasonal changes that normally make it difficult to detect true ecological changes in these environments.
- To check how accurate the vegetation maps and change detection findings are by comparing them with reliable reference data from multiple sources including very detailed satellite images from Google Earth Pro (Loew et al., 2017).
- To explain the observed vegetation changes by connecting satellite data with natural ecological processes and human activities (Yue et al., 2024). The research will develop practical, evidence supported recommendations for managing Miombo woodlands sustainably in ways that align with current international conservation agreements and frameworks.

2. LITERATURE REVIEW

Miombo woodlands thrive in areas with very definite wet and dry seasons. They receive between 650-1,400 mm of intense rain during a wet season that lasts only 5-7 months of the year (Frost, 1996). Before the rainy season begins, Miombo trees start growing new leaves, a process called pre-rain greening. During the dry season most trees in this woodlands lose their leaves but they have adapted to sprout new leaves even before the first rain arrive (Vinya et al., 2019). The vegetation structure of Miombo woodlands consists of a single-story tree canopy that typically covers 70% of the ground with tree heights ranging from 10-20 meters (Kutsch et al., 2011). The area below the tree canopy comprises of grasses, flowering plants, and small shrubs which gives the ecosystem a savanna-like appearance. Fire plays a natural role in this environment, with most areas experiencing burns every 1-3 years primarily during the late dry season (Meneses et al., 2024). Miombo woodlands contain fewer species than tropical rainforests but have many unique plants found nowhere else in the world. They are home to about 8,500 plant species, and remarkably over 54% only exist in this region (Timberlake & Chidumayo, 2011). The rich variety of plant and animal life in these woodlands has developed over years alongside human communities. This long history of coexistence has created an ecosystem that can withstand certain human activities and in some cases, actually relies on human practices to maintain its natural balance. Miombo woodlands constantly change due to both natural forces and human influences. These ecosystems are not static but respond and adapt to different pressures over time. Having a clear understanding of how and why these woodlands change is essential for protecting them while still allowing people to use their resources in suitable ways (Ribeiro et al., 2020).

2.1 Natural Factors Affecting Vegetation Change

Several natural factors influence vegetation dynamics in Miombo woodlands:

- **Climate Variability** – Rainfall patterns strongly influence vegetation productivity and distribution. Drought periods can lead to tree mortality and shifts in species composition (Mureva et al., 2024). In savannas with less than 650 mm annual rainfall, tree cover is primarily limited by water availability, while areas with higher rainfall are maintained as open woodlands largely through disturbances like fire (Staver et al., 2011).
- **Fire Regimes** – Fire plays a critical ecological role in Miombo systems. While many Miombo tree species have adaptations to survive frequent burning, changes in fire

frequency or intensity can alter woodland structure (Ryan & Williams, 2011). Frequent late-season fires tend to promote a more open woodland structure by killing small trees and preventing recruitment to larger size classes (Meneses et al., 2024).

- **Wildlife Interactions** – Herbivores influence vegetation structure through browsing and grazing, which can either promote or inhibit tree recruitment depending on intensity (Staver & Bond, 2014). Large animals like elephants can cause significant structural changes through their feeding habits, particularly during drought periods (Thornley et al., 2020).

2.2 Anthropogenic Drivers of Vegetation Change

Human activities significantly impact Miombo woodland dynamics:

- **Agricultural Expansion** - Conversion of woodland to cropland is one of the primary drivers of Miombo deforestation. Small-scale subsistence farming and larger commercial agriculture both contribute to this process (Nogueira Lisboa et al., 2024). After abandonment, fields may regenerate into secondary woodland, but the species composition typically differs from mature Miombo (Montfort et al., 2021).
- **Charcoal Production** - Charcoal remains the dominant cooking fuel throughout much of the Miombo region. In Zambia, charcoal production alone contributes to almost a quarter of the country's deforestation, with 300,000 hectares of forests lost each year due to tree felling (Smith, 2021).
- **Timber Extraction** - Selective logging of valuable hardwood species like *Pterocarpus angolensis* and *Dalbergia melanoxylon* alters forest structure and composition (Modest et al., 2011). While less visibly destructive than clear-cutting, selective logging can lead to progressive degradation, particularly when combined with other disturbances (Osazuwa-Peters et al., 2015).
- **Altered Fire Regimes** - Human-induced changes to fire regimes, including increased fire frequency or shifts in seasonal timing, can significantly impact woodland structure (Hagmann et al., 2021; Nguyen et al., 2023). Late dry season fires, in particular, can be more intense and damaging to tree cover than early dry season fires (Ryan & Williams, 2011).

Figure 1 below shows drivers of forest change by district in the Miombo woodlands of southeastern Tanzania.

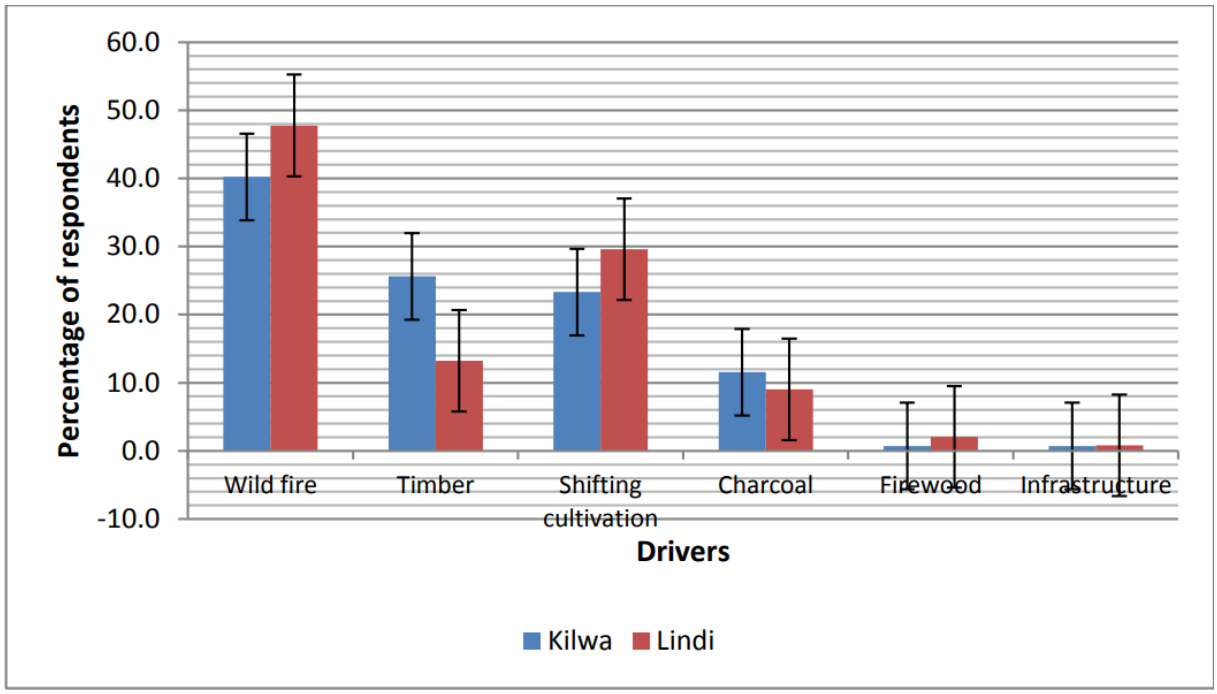

Figure 1: Drivers of Forest Change by District

Source:(Kulindwa et al., 2016)

2.3 Remote Sensing of Vegetation

Satellite remote sensing has evolved substantially since the launch of the first Landsat satellite in 1972, with significant advancements in spatial, spectral, temporal, and radiometric resolutions enabling increasingly sophisticated analyses of land cover and vegetation dynamics (Phiri & Morgenroth, 2017). For Miombo woodlands, the Landsat program has provided particularly valuable historical data, with its 30m spatial resolution capturing woodland structure at scales relevant to management and policy implementation (Useni Sikuzani et al., 2024).

The advent of medium-resolution sensors such as MODIS (Moderate Resolution Imaging Spectroradiometer) in the early 2000s revolutionized vegetation monitoring by providing daily observations at 250-1000m resolution, enabling detailed analysis of seasonal phenology and interannual variability across large geographic areas (Ulsig et al., 2017; X. Zhang et al., 2003). While the coarser spatial resolution of MODIS limits its utility for detecting small-scale disturbances common in Miombo landscapes, its high temporal frequency has proven valuable for characterizing seasonal vegetation dynamics and identifying anomalies indicative of potential (Anyamba et al., 2003).

More recently, the European Space Agency's Sentinel program, particularly Sentinel-2 launched in 2015, has further enhanced capabilities for woodland monitoring through improved spatial resolution (10-20m), strategic positioning of spectral bands, and more frequent revisit intervals compared to Landsat (Runge & Grosse, 2019). These advancements have enabled more detailed characterization of woodland structure and composition, as well as improved detection of gradual changes associated with degradation processes (López-Amoedo et al., 2021).

2.3.1 Optical Remote Sensing for Vegetation Analysis

Remote sensing has become an essential tool for monitoring vegetation changes in woodland ecosystems, providing systematic observations over large areas and through time (Darabi et al., 2025).

- **Vegetation Indices** - Normalized Difference Vegetation Index (NDVI) and Enhanced Vegetation Index (EVI) are commonly used to assess vegetation greenness and productivity. These indices exploit the contrast between red light absorption by chlorophyll and near-infrared reflection by plant cell structures (Didan, 2015). In Miombo woodlands, NDVI has been shown to correlate with tree cover and biomass, though saturation can occur in denser areas (Basalumi et al., 2018).
- **Red-Edge Indices** - Sentinel-2's red-edge bands offer enhanced capabilities for vegetation monitoring. Indices like Normalized Difference Red-Edge (NDRE) and Sentinel-2 Red-Edge Position (S2REP) have shown improved sensitivity to canopy chlorophyll content and can better differentiate subtle changes in woodland structure (Frampton et al., 2013).
- **Classification Approaches**: Land cover classification techniques identify different vegetation types and densities. Supervised classification methods like Random Forest have proven effective for mapping Miombo woodland types when training data is available. Object-based approaches that consider spatial context alongside spectral information can improve classification accuracy in heterogeneous landscapes like Miombo woodlands (Nkya et al., 2024a).

2.3.2 Change Detection Methodologies

Several approaches are used to detect and quantify vegetation changes from satellite imagery. Bi-temporal Analysis approach compares images from two distinct time periods to identify changes. Post-classification comparison involves independently classifying images from different dates and then comparing the resulting maps (El-Hattab, 2016). Image differencing represent the most straightforward bi-temporal approaches, involving pixel-by-pixel subtraction or division of values from two dates, typically using vegetation indices such as NDVI rather than raw spectral bands (Alphan, 2013). These methods produce continuous measures of change magnitude, which must be thresholded to identify significant changes. While conceptually simple and computationally efficient, these approaches are highly sensitive to phenological differences, atmospheric conditions, and sensor calibration issues, potentially leading to false change detection (Panuju et al., 2020). Change Vector Analysis method tracks changes in multiple dimensions (e.g., brightness and greenness) simultaneously, providing information on both the magnitude and direction of change (Carvalho Júnior et al., 2011). Applications in Miombo contexts have demonstrated CVA's utility for detecting subtle disturbances such as selective harvesting that may be missed by simpler approaches (Kissanga et al., 2024). Time series analysis approaches like BFAST (Breaks For Additive Season and Trend) decompose time series of satellite observations into seasonal, trend, and remainder components to detect abrupt changes and gradual trends (Watts & Laffan, 2014). These methods can help distinguish long-term woodland degradation from seasonal fluctuations (Gao et al., 2021).

2.4 Advantages of Sentinel-2 for Woodland Monitoring

The European Space Agency's Sentinel-2 mission offers several advantages for monitoring Miombo woodlands. With enhanced spatial resolution of 10-meter in key bands, Sentinel-2 provides more detailed imagery than the 30-meter resolution of Landsat, enabling detection of smaller-scale disturbances and more precise mapping of woodland boundaries (Phiri et al., 2020). Sentinel-2's three red-edge bands (at 705, 740, and 783 nm) are particularly valuable for vegetation analysis. These bands provide enhanced sensitivity to chlorophyll content and canopy structure compared to traditional multispectral sensors (Qiao et al., 2024). Studies have shown that red-edge indices can better differentiate woodland types and detect subtle degradation than standard NDVI (Liu et al., 2024).

2.5 Google Earth Engine for Large-Scale Environmental Monitoring

Google Earth Engine (GEE) represents a significant advancement in how remote sensing data is processed and analyzed, particularly for large-scale environmental monitoring. GEE provides a cloud-based platform that eliminates the need for local processing of large satellite datasets, enabling analyses that would be computationally prohibitive on personal computers (Gorelick et al., 2017). The platform hosts a multi-petabyte catalog of satellite imagery and geospatial datasets, including the complete Sentinel-2 archive, accessible without the need for downloading or storing data locally (Schmitt et al., 2019). The platform's JavaScript API allows users to develop and run algorithms that operate on the entire data catalog, with the code-based approach enabling reproducible analyses and facilitating sharing of methodologies (Berra et al., 2024). Several studies have demonstrated GEE's effectiveness for woodland monitoring in Africa (Anchang et al., 2020). GEE was used for regional land cover mapping in Southeast Asia, demonstrating approaches applicable to Miombo regions (Macarringue et al., 2023).

2.6 Challenges in Remote Sensing

Despite technological advances, several challenges remain in remote sensing of Miombo ecosystems. The strong seasonality of Miombo woodlands creates challenges for consistent monitoring, as leaf shedding during the dry season can lead to underestimation of woody cover if images from different phenological stages are compared (Nkya et al., 2024b). The heterogeneous nature of Miombo landscapes, with their mixture of trees, shrubs, and grasses, creates mixed pixels that can be difficult to classify accurately, particularly at coarser resolutions (Nghiyalwa et al., 2021). Persistent cloud cover during the wet season limits the availability of optical imagery for certain periods, creating temporal gaps in observations (Rahimi & Jung, 2024). Additionally, different degradation processes can produce similar spectral signatures, making it challenging to distinguish between different types of woodland change using only spectral information (Heydari & Fatemi Nasrabadi, 2023).

2.7 Research Gap and Contribution

While numerous studies have examined vegetation changes in African savanna and woodland ecosystems, specific applications of Sentinel-2's enhanced capabilities for Miombo woodland monitoring remain relatively limited. The unique spectral properties of Sentinel-2, particularly

its red-edge bands, offer potential improvements in detecting and characterizing subtle changes in woodland structure that traditional indices and sensors might miss (Mutowo, 2018). most previous studies have focused on either dense forests or open savannas, with less attention to the intermediate woodland systems like Miombo. These ecosystems often show more complex responses to disturbances, with potential degradation pathways that may not be adequately captured by conventional methods developed for other ecosystem types (Bhattarai et al., 2020).

This study aims to address these gaps by systematically comparing the performance of traditional and red-edge-based indices for characterizing Miombo woodland changes, and by developing an approach specifically tailored to the structural and phenological characteristics of these important ecosystems.

3. METHODOLOGY

3.1 Overview

This chapter outlines the methodological framework employed to assess changes in vegetation structure and condition in the Miombo woodlands using remotely sensed data. The approach is primarily based on Sentinel-2 imagery, which provides high-resolution multispectral data suitable for vegetation monitoring.

Level-2A (L2A) Sentinel-2 surface reflectance products were utilized to ensure accuracy and consistency in detecting environmental changes. The L2A data products are atmospherically corrected, ensuring minimal atmospheric interference and enabling reliable comparisons across temporal datasets. Sentinel-2 images for two distinct time periods—May 2017 to April 2018 and May 2022 to April 2023—were selected to investigate landscape transitions and vegetation dynamics over five years.

The methodological process incorporated several critical steps:

- **Data Acquisition and Preprocessing:** Collection of Sentinel-2 imagery, cloud masking, and reflectance scaling.
- **Vegetation Indices Calculation:** Derivation of the Normalized Difference Vegetation Index (NDVI) and Enhanced Vegetation Index (EVI) for vegetation analysis.
- **Vegetation Classification:** Classifying vegetation condition using threshold-based categorizations derived from NDVI and EVI.
- **Change Detection Analysis:** Identifying spatial patterns of vegetation change through class transitions and index differencing.
- **Statistical Analysis:** Conducting zonal statistics to quantify area changes, accompanied by accuracy assessment using confusion matrices and stratified sampling validation.

3.2 Study Area

This study focused on a 1-degree by 1-degree area (approximately 12,047 square kilometers) located in eastern Zambia (31.5°E to 32.5°E, -13.5°S to -12.5°S), within the broader Miombo woodland ecoregion. This area was selected because it contains representative Miombo woodland vegetation with varying degrees of human impact and natural variation.

The study area experiences a tropical continental climate with three distinct seasons: a hot dry season (September-November), a hot wet season (December-April), and an incredible dry season (May-August). Annual rainfall averages 800-1000 mm, concentrated in the wet season. The region is characterized by gently undulating topography with elevations ranging from approximately 500 to 1000 meters above sea level. Figure 2 below shows the study area of research.

GEE codes used were:

var studyArea = ee.Geometry.Rectangle([31.5, -13.5, 32.5, -12.5]);

Map.centerObject(studyArea, 9);
Map.addLayer(studyArea, {color: 'red'}, 'Study Area');

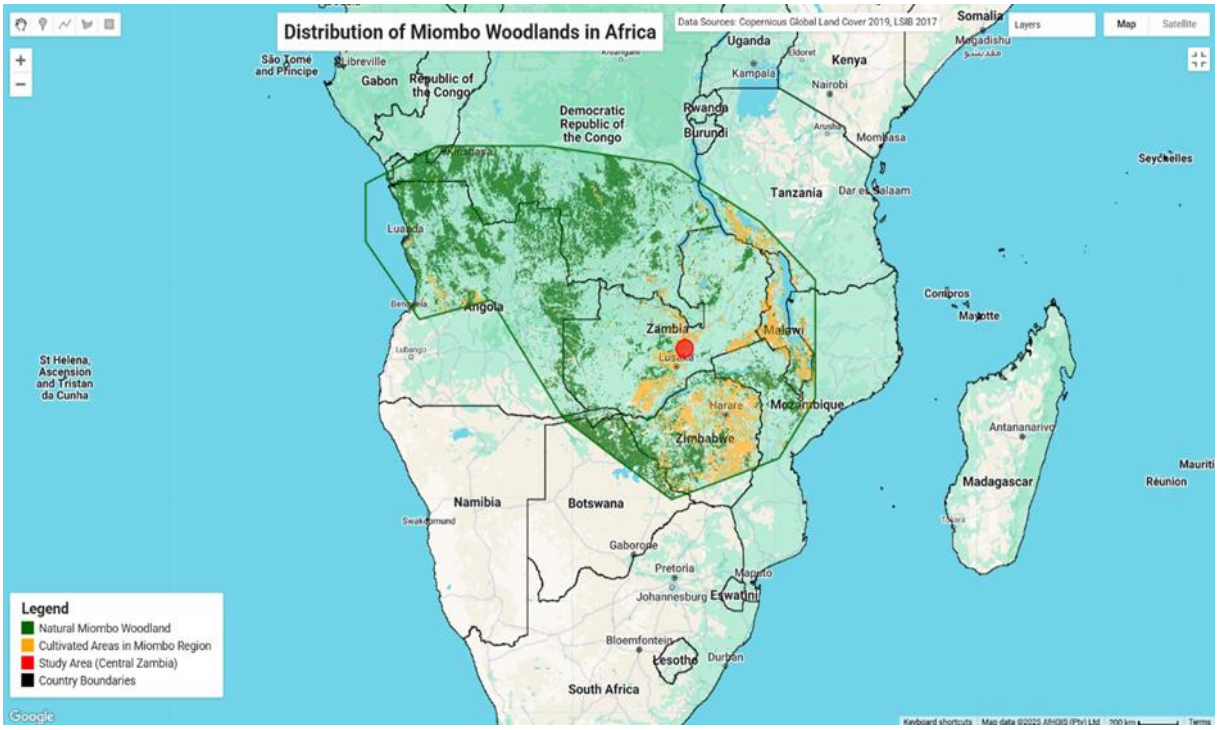

Figure 2: Study area (Central Zambia)

Source: Author's work created using GEE

3.3 Data Acquisition and Pre-Processing

Satellite Data Selection - Sentinel-2 imagery was selected from the Copernicus program archives:

- Baseline period (2017–2018): Level-1C (L1C) top-of-atmosphere imagery.
- Recent period (2022–2023): Level-2A (L2A) surface reflectance imagery.

This distinction was critical due to changes in the Sentinel-2 processing baseline. Earlier L1C imagery required traditional scaling, while newer L2A imagery introduced an offset in reflectance calculations.Sentinel-2 bands with 10-meter resolution (B2, B3, B4, B8) were used for vegetation analysis. Red-edge and SWIR bands were not primary inputs but were considered for future study.

Two time periods were selected for analysis - Baseline period from May 2017 to April 2018, and Recent period from May 2022 to April 2023. These periods were chosen to provide a five-year interval for change detection long enough to detect meaningful ecological changes. Within each period, images from the late dry season were prioritized because Cloud cover is minimal during this season in the study area, phenological conditions are relatively stable, and the contrast between woody vegetation and the understory is maximized, as most grasses are dry while woody plants retain some greenness. (Y. Cheng et al., 2020; Van Passel et al., 2020).

GEE codes used:

```
var period1718 = { start: '2017-05-01', end: '2018-04-30' };
var period2223 = { start: '2022-05-01', end: '2023-04-30' };
```

3.4 Google Earth Engine Processing

All data processing was conducted using Google Earth Engine (GEE), a cloud-based platform for planetary-scale geospatial analysis. GEE provides access to the full archive of Sentinel-2 imagery and offers the computational power needed to process large datasets efficiently (Lasaponara et al., 2022). Reflectance scaling for Sentinel-2 imagery was implemented following guidelines provided by the European Space Agency (ESA) Copernicus Sentinel-2 mission, with considerations based on the processing baseline used for each dataset. For the Level-1C (L1C) products from the years 2017 to 2018, reflectance values were derived by scaling the digital numbers (DN) by a factor of 10,000, following the established ESA standards (ESA, 2015; ESA, 2017). The formula applied for this conversion is as follows:

For L1C data (2017–2018), reflectance was calculated by dividing digital numbers (DN) by 10,000: Reflectance = DN/10000.

For L2A data (2022–2023), a radiometric offset introduced in Processing Baseline 04.00 and above was considered: Reflectance = (DN-1000) / 10000 (Delwart, 2015; Doxani et al., 2018).

3.5 Cloud Masking and Composite Creation

To minimize the impact of clouds on the analysis, two filtering steps were applied, images with greater than 50% cloud cover were excluded and a cloud mask to remove clouds and cloud shadows from the remaining images.

Cloud masking was performed using the QA60 quality assessment band for LC1 and the SCL band for L2A to remove cloudy pixels.

For L1C cloud masking:

var qa = image.select('QA60');

var mask = qa.bitwiseAnd(1 << 10).eq(0).and(qa.bitwiseAnd(1 << 11).eq(0));

For L2A cloud masking:

var scl = image.select('SCL');

var mask = scl.neq(3).and(scl.neq(8)).and(scl.neq(9)).and(scl.neq(10));

After cloud filtering and masking, median composites were created for each time period. The median composite approach was chosen because it effectively removes remaining cloud artifacts and other anomalies while preserving the overall spectral characteristics of the landscape (*Generating Composite Images — Digital Earth Africa 2021 Documentation*, 2021).

GEE codes used:

Var composite = filteredCollection.median();

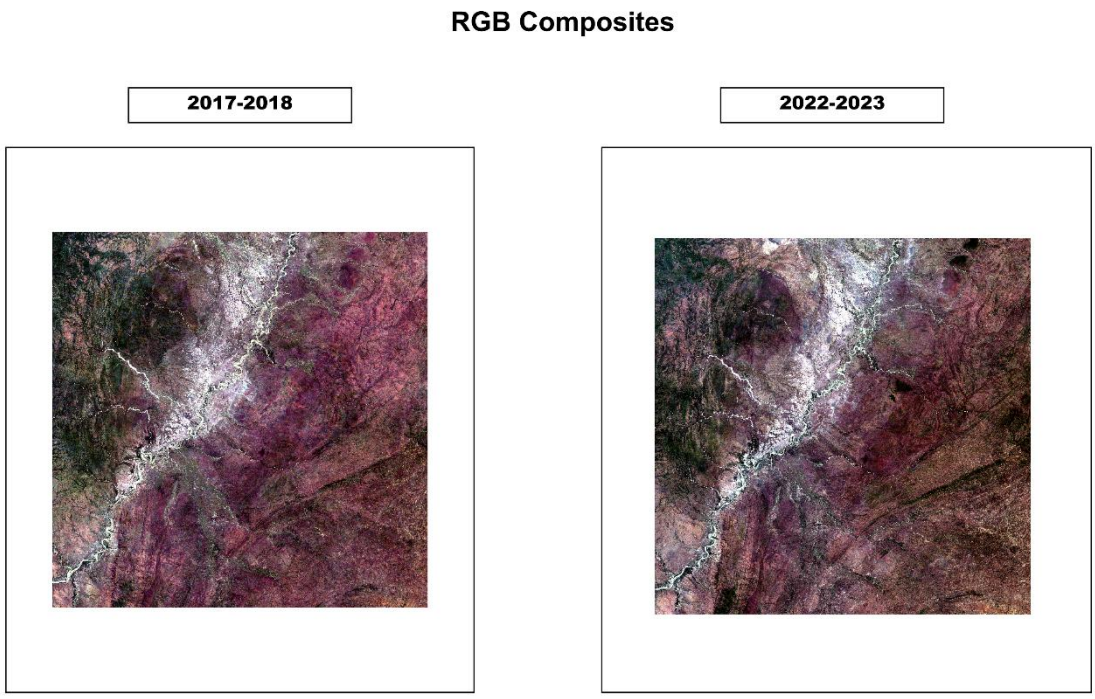

Figure 3: RGB composite for both periods

Source: Author's own creation

3.5.1 Vegetation Indices Calculation

For this study, I calculated two different vegetation indices to characterize vegetation structure and condition: the Normalized Difference Vegetation Index (NDVI) and the Enhanced Vegetation Index (EVI). Using two complementary indices allowed me to compare their effectiveness for detecting vegetation changes in Miombo woodland ecosystems.

3.5.1 NDVI Calculation

Normalized Difference Vegetation Index (NDVI): This widely used index measures the contrast between near-infrared reflection (which vegetation strongly reflects) and red light absorption (which chlorophyll absorbs). NDVI ranges from -1 to +1, with higher values indicating denser green vegetation (Li et al., 2021). NDVI was calculated using the formula NDVI = (NIR - Red) / (NIR + Red). In Google Earth Engine, this was implemented as:

var ndvi = composite.normalizedDifference(['B8', 'B4']).rename('NDVI');

3.5.2 EVI Calculation

The Enhanced Vegetation Index (EVI) was developed to address some of the limitations of NDVI, particularly in areas with dense vegetation where NDVI can saturate and in regions where soil background can influence vegetation readings. EVI incorporates the blue band to correct for atmospheric influences and includes coefficients to adjust for soil background effects (Huete et al., 2002). The formula for EVI is EVI = 2.5 × ((NIR - RED) / (NIR + 6 × RED - 7.5 × BLUE + 1))

GEE codes used:

```
var evi = composite.expression(
  '2.5 * ((NIR - RED) / (NIR + 6 * RED - 7.5 * BLUE + 1))', {
    'NIR': composite.select('B8'),
    'RED': composite.select('B4'),
    'BLUE': composite.select('B2')
}).rename('EVI');
```

3.6 Vegetation Classification

3.6.1 NDVI Threshold-Based Classification

A threshold-based classification approach was applied to the NDVI data to characterize vegetation structure across the landscape. This approach classified the landscape into four vegetation classes based on NDVI values:

- Bare soil/Non-vegetated areas (NDVI < 0.2)
- Sparse vegetation/Grassland (0.2 ≤ NDVI < 0.4)
- Open woodland (0.4 ≤ NDVI < 0.6)
- Dense woodland (NDVI ≥ 0.6)

These NDVI threshold values represent different levels of photosynthetic activity and vegetation density. The lowest values (below 0.2) typically indicate areas with little to no vegetation, such as bare soil, rock, or built environments. As NDVI increases, so does the density and health of vegetation. Values between 0.2 and 0.4 represent areas with some

vegetation but limited coverage, typical of grasslands or very sparse woodlands. The middle range (0.4-0.6) captures open woodland areas where trees are present but not forming a closed canopy. The highest values (above 0.6) indicate dense woodland areas with substantial tree cover and active photosynthesis (*NDVI, the Foundation for Remote Sensing Phenology | U.S. Geological Survey*, 2018; Walz & Weber, 2021).

GEE codes used:

```
function classifyNDVI(ndvi) {
  return ndvi.expression(
    'NDVI < 0.2 ? 1 : NDVI < 0.4 ? 2 : NDVI < 0.6 ? 3 : 4',
    {'NDVI': ndvi}).rename('Veg_Class');
}
var vegClass1718 = classifyNDVI(ndvi1718);
var vegClass2223 = classifyNDVI(ndvi2223);
```

The classification rules based on NDVI index ranges are summarized in Table 1.

Index Range	Class Name	Class Code
< 0.2	Bare / Non-Vegetated	1
0.2 - 0.4	Sparse Vegetation	2
0.4 - 0.6	Open Woodland	3
> 0.6	Dense Woodland	4

Table 1: NDVI Threshold classification rule

Source: Author's own work

3.6.2 EVI Threshold Based Classification

The Enhanced Vegetation Index (EVI) values generally run lower than NDVI values for the same vegetation conditions, which is why thresholds for EVI were defined using slightly lower numerical ranges. This difference arises because EVI is specifically designed to be more

sensitive in areas with dense vegetation, where NDVI tends to saturate, and it also reduces the influence of soil background and atmospheric effects (Huete et al., 2002).

For example, a place that shows 0.6 on the NDVI scale (dense woodland) might only show 0.45 on the EVI scale. This study used lower thresholds for EVI to ensure the vegetation classes still match between the two indices. Areas with EVI below 0.15 were classed as bare, 0.15 to 0.35 as sparse vegetation, 0.35 to 0.50 as open woodland, and above 0.50 as dense woodland. These cutoffs match how EVI behaves and allow for a fair comparison with NDVI results.

This approach ensures that the comparison between NDVI and EVI results reflects actual ecological differences rather than differences caused by index scaling. The classification rules are summarized in Table 2.

GEE codes used:

```
function classifyEVI(evi) {
  return evi.expression(
    'EVI < 0.15 ? 1 : EVI < 0.35 ? 2 : EVI < 0.5 ? 3 : 4',
    {'EVI': evi}
  ).rename('EVI_Veg_Class');
}
var eviClass1718 = classifyEVI(evi1718);

var eviClass2223 = classifyEVI(evi2223);
```

The classification rules based on EVI index ranges are summarized in Table 2.

Index Range	Class Name	Class Code
< 0.15	Bare / Non-Vegetated	1
0.15 – 0.35	Sparse Vegetation	2
0.35 – 0.50	Open Woodland	3
> 0.50	Dense Woodland	4

Table 2: EVI Threshold classification rule

Source: Author's work

3.7 Supervised Classification Using Random Forest

A supervised machine learning approach using the Random Forest (RF) algorithm was implemented in Google Earth Engine (GEE) to improve vegetation classification accuracy and address the limitations of earlier threshold-based methods. This section outlines the procedures for developing and validating the Random Forest classifier using multi-index and multi-band feature data.

3.7.1 Motivation and Limitations of Threshold Classification

The initial vegetation classification approach utilized threshold-based rules for NDVI and EVI indices to assign vegetation classes based on fixed value ranges. Although this method provided a straightforward and computationally efficient means of classifying vegetation cover, it was limited in capturing the complexity of heterogeneous landscapes such as the Miombo woodlands. Threshold-based methods are inherently sensitive to spectral overlap between vegetation types, background noise, and seasonal variability, often leading to classification inaccuracies.

To address these shortcomings, a supervised classification approach based on the Random Forest (RF) algorithm was implemented. The Random Forest model utilized a broader set of input features, including spectral bands and vegetation indices such as NDVI and EVI, allowing for a more nuanced, data-driven classification that better captured the structural and phenological diversity of the landscape.

3.7.2 Ground Truth Data Collection and Preprocessing

Ground truth samples were generated manually using high-resolution imagery in Google Earth Pro to support supervised classification and accuracy assessment. This approach allowed the identification and labeling of vegetation classes based on visual interpretation, ensuring that samples accurately reflected real-world vegetation conditions.

Validation points were collected across the study area for the 2017 baseline period, with each point assigned one of four vegetation classes: Very Low Vegetation, Low Vegetation, Moderate

Vegetation, or High Vegetation. Care was taken to distribute points across different vegetation types and geographic regions, minimizing spatial bias.

The collected points were exported as a CSV file and imported into Google Earth Engine (GEE) for use in classification validation. Figure 4 illustrates the location and distribution of the manually collected ground truth points across the study landscape.

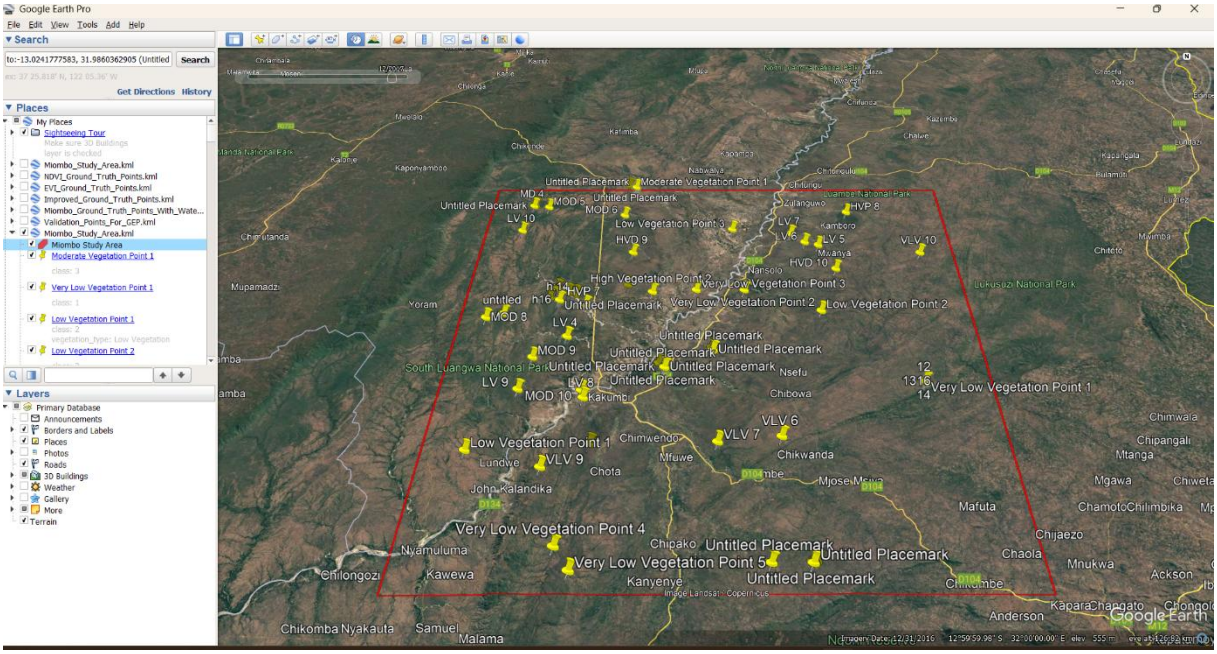

Figure 4: Distribution of vegetation validation points in study area

Source: Validation points collected by Author. Background imagery from Google Earth

3.8 Change Detection

3.8.1 NDVI Change Detection

The first change detection approach involved comparing the vegetation classifications from the two time periods. This post-classification comparison technique identifies specific transitions between vegetation classes (e.g., from dense woodland to sparse vegetation). With this approach, each pixel in the resulting map has a value that represents its transition. For example, a value of 11 indicates bare soil in both periods (no change), while a value of 43 indicates a change from dense woodland to open woodland (degradation). Similarly, a value of 24 indicates a change from sparse vegetation to dense woodland (regeneration) (Peiman, 2011). This detailed transition map was visualized using a color scheme that highlights different types of

transitions, making distinguishing between areas of stability, degradation, and recovery across the landscape easier.

var changeMap = vegClass1718.multiply(10).add(vegClass2223).rename('Change_Map');

3.8.2 EVI Change Detection

The second change detection approach focused on analyzing changes in the Enhanced Vegetation Index (EVI) between the two time periods. Similar to the NDVI-based approach, this method helps identify areas with significant changes in vegetation productivity. The code "*var eviChangeMap = eviClasses.multiply(10).add(eviClassesRecent);*" creates a transition map where each pixel's value represents how vegetation has changed over time. For example, a value of 11 indicates very low EVI in both periods (persistently non-vegetated areas), while a value of 43 indicates a change from high EVI to moderate EVI (slight vegetation degradation). Similarly, a value of 24 indicates a change from low EVI to high EVI (significant vegetation regeneration) (Zhu et al., 2016). This detailed EVI transition map was visualized using a color scheme that highlights different types of transitions in vegetation productivity, making it easier to interpret the patterns of change across the landscape.

GEE code used:

var eviChangeMap = eviClass1718.multiply(10).add(eviClass2223).rename('EVI_Change_Map');

3.8.3 Change Direction Analysis

To simplify the interpretation of changes, a change direction map was created that classified changes into three main categories: stable areas (no change in class), vegetation loss (decrease in class value), and vegetation gain (increase in class value).

This simplified categorization helps us see the bigger picture of landscape changes without getting lost in the details of specific transitions. Rather than tracking precisely which class changed to which other class, this approach focuses on the fundamental question: is an area gaining vegetation, losing vegetation, or staying relatively consistent?

The stable areas represent ecosystem consistency places where the vegetation structure remained unchanged during our study period. Vegetation loss areas indicate locations experiencing degradation, deforestation, or other processes that reduce plant cover. Vegetation

gain areas show locations of ecological recovery, reforestation, or other positive vegetation changes.

GEE code used:

```
var changeDirection = ee.Image(0)
  .where(vegClass1718.eq(vegClass2223), 1)
  .where(vegClass1718.gt(vegClass2223), 2)
  .where(vegClass1718.lt(vegClass2223), 3)
  .rename('Change_Direction');
var eviChangeDirection = ee.Image(0)
  .where(eviClass1718.eq(eviClass2223), 1)
  .where(eviClass1718.gt(eviClass2223), 2)
  .where(eviClass1718.lt(eviClass2223), 3)
  .rename('EVI_Change_Direction');
```

3.8.4 Index Difference Analysis

In addition to the categorical change detection approaches, a continuous measure of change was calculated by directly subtracting the index values from the two time periods. For NDVI. I used the code ‘‘*var ndviDiff = ndvi2223.subtract(ndvi1718).rename('NDVI_Diff')*’’ to calculate the difference. For EVI, I used ‘‘*var eviDiff = evi2223.subtract(evi1718).rename('EVI_Diff');*’’ to find the change between periods. This continuous approach offers several advantages over the categorical methods. While the classification-based approaches tell us when a pixel crosses a threshold (like changing from "open woodland" to "dense woodland"), the difference maps reveal the actual magnitude of change, capturing subtle variations that might not trigger a class change. For example, an area classified as "open woodland" in both periods might still show significant improvement or degradation within that category.

The NDVI and EVI difference maps were visualized using diverging color palettes where red indicates vegetation loss, yellow indicates minimal change, and green indicates vegetation gain.

This intuitive color scheme makes it immediately apparent where vegetation is declining, improving, or remaining stable across the landscape.

3.9 Feature Construction: Spectral Bands and Vegetation Indices

Each composite image for 2017–2018 and 2022–2023 was enhanced by computing vegetation indices to enrich the feature space. The following features were used:

- Sentinel-2 spectral bands: B2 (Blue), B3 (Green), B4 (Red), B8 (Near-Infrared)
- NDVI (Normalized Difference Vegetation Index)
- EVI (Enhanced Vegetation Index)
- SAVI (Soil-Adjusted Vegetation Index)

The final feature stack contained seven bands: *var bands = ['B2', 'B3', 'B4', 'B8', 'NDVI', 'EVI', 'SAVI'];*

3.9.1 Model Training and Classification

The Random Forest (RF) classifier was trained using manually collected ground truth points derived from high-resolution Google Earth Pro imagery. The validation points were assigned to four vegetation classes: Very Low, Low, Moderate, and High Vegetation, ensuring a representative coverage of the study area.

The RF model was configured with 100 decision trees to balance model robustness with computational efficiency. The ground truth points were uploaded into Google Earth Engine (GEE), and the Random Forest training process was implemented as follows:

```
var classifier = ee.Classifier.smileRandomForest(100)
 .train({
  features: trainingSamples,
  classProperty: 'Class',
  inputProperties: bands
 });
```

Once trained, the model was applied to classify the 2017–2018 and 2022–2023 composite feature images, generating vegetation class maps for both periods.

3.9.2 Accuracy Assessment via Cross-Validation

To assess model performance, the ground truth dataset was split into:

- 80% for training
- 20% for validation

The validation subset was classified using the trained RF model, and the predictions were compared to reference labels to generate a confusion matrix.

```
var rfConfMatrix = validation.errorMatrix('Class', 'classification');

print(rfConfMatrix.accuracy());

print(rfConfMatrix.kappa());
```

3.9.3 Statistical Analysis and Validation

Zonal statistics were computed to quantify area changes between the two classified periods. Pixel-based area calculations were performed within GEE, summarizing the total area occupied by each vegetation class in hectares.

GEE code for area calculation:

```
var pixelArea = ee.Image.pixelArea();
var statsNDVI1718 = pixelArea.addBands(vegClass1718).reduceRegion({
  reducer: ee.Reducer.sum().group({groupField: 1, groupName: 'class'}),
  geometry: studyArea,
  scale: 10,
  maxPixels: 1e9
});
```

This statistical analysis enabled precise quantification of vegetation stability, degradation, and regrowth dynamics over the six-year study period. Figure 5 below shows the Workflow Pipeline.

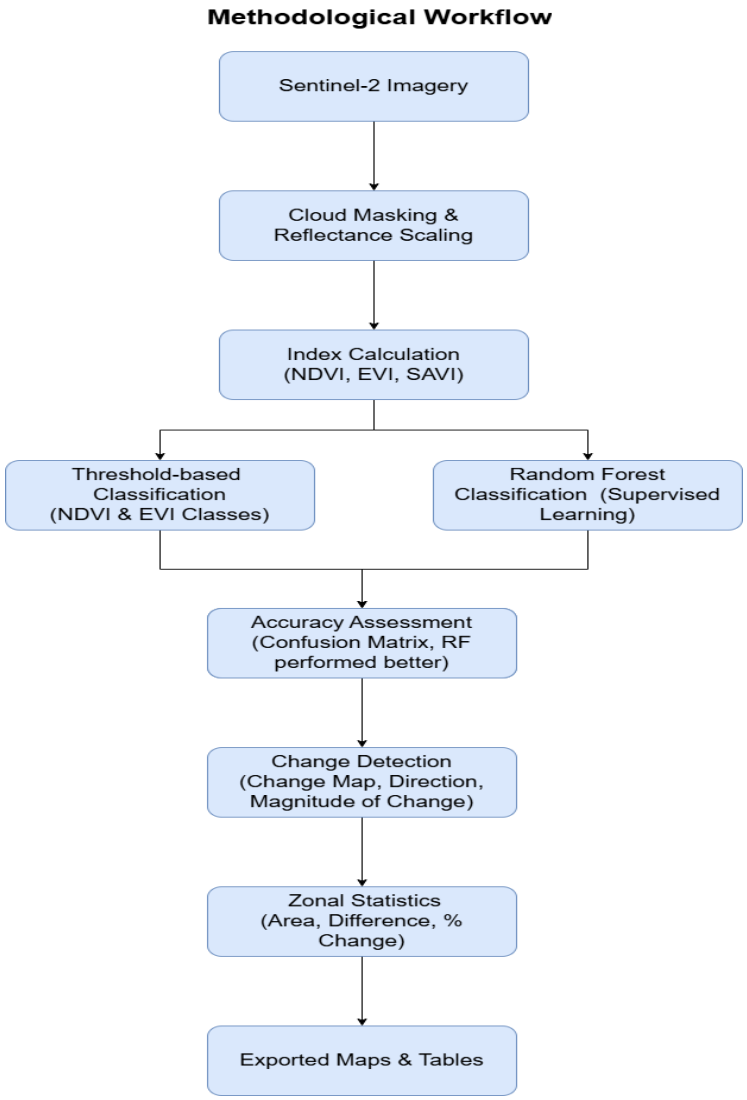

Figure 5: Methodological workflow for vegetation change analysis

Source: Author's work

4. RESULTS

This chapter presents the spatial and temporal changes in vegetation across the Miombo woodland study area, using NDVI and EVI outputs derived from Sentinel-2 imagery. Results include base-year and current-year vegetation conditions, vegetation classifications, index difference layers, change direction maps, and vegetation class transitions. Both NDVI and EVI outputs are presented in a parallel structure to enable side-by-side interpretation.

4.1 Vegetation Index Composites

Vegetation greenness is a widely used proxy to assess vegetation health, productivity, and cover using satellite-derived indices. In this study, the Normalized Difference Vegetation Index (NDVI) and the Enhanced Vegetation Index (EVI) were both applied over two different composite periods (2017–2018 and 2022–2023) to visualize and analyze spatial patterns in vegetation density and vigor across the Miombo woodland landscape. Figures 6 and 7 compare the NDVI and EVI composites for each time period.

The NDVI map shows denser vegetation (values approaching 0.8) distributed throughout the central and southern parts of the study area. These darker green regions represent healthy, photosynthetically active vegetation, characteristic of intact woodland canopies. Areas of relatively lower NDVI, evident in yellow to light green shades, occur along riverine corridors and peripheral regions, likely reflecting agricultural lands, built-up areas, or degraded woodland.

Similarly, the EVI composite captures comparable patterns, but with generally lower maximum values (up to 0.7). EVI's sensitivity to canopy structure and its resistance to atmospheric distortions makes it especially useful in distinguishing subtle variations within densely vegetated areas. In Figure 6, the EVI map reflects more detail in highly vegetated patches and some of the moderate-to-low vegetation gradients than NDVI. Overall, both indices affirm a relatively healthy and extensive vegetation cover for 2017–2018, though EVI provides slightly smoother gradients and refined contrast in greener patches.

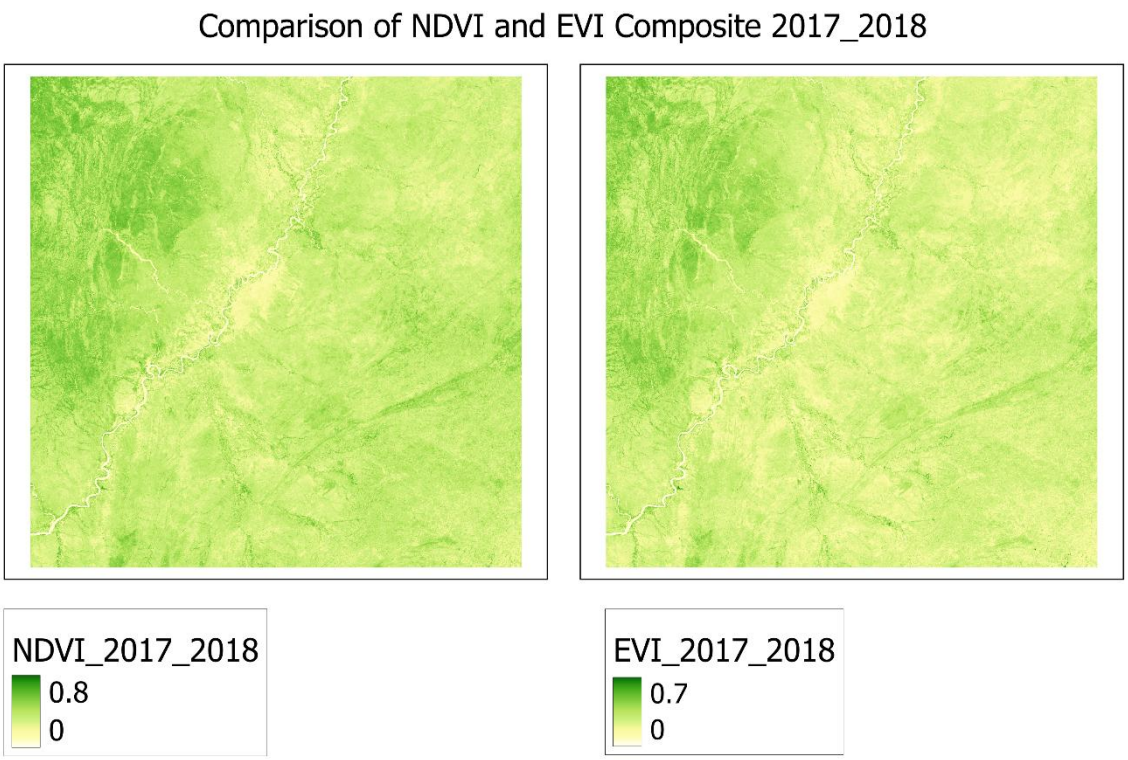

Figure 6: Comparison of NDVI and EVI composite images for the 2017–2018 period

Source: Author's own work

Figure 7 presents the NDVI and EVI composite maps for the 2022–2023 period, providing a snapshot of vegetation conditions across the Miombo woodland study area. The visual comparison highlights distinct patterns between the two vegetation indices in representing landscape greenness and structure.

The NDVI composite map (Figure 7, left) predominantly displays lighter tones of green, with NDVI values ranging from 0 to approximately 0.8. Most of the landscape exhibits lower NDVI values, particularly concentrated in the 0.2 to 0.4 range, suggesting moderate to sparse vegetation cover. These lighter tones could indicate widespread disturbances, woodland degradation, land-use changes, or a reduction in vegetation productivity influenced by climatic variability or anthropogenic pressures. Riverine zones and some isolated patches demonstrate slightly higher NDVI values, yet large portions of the area reflect subdued greenness.

In contrast, the EVI composite map (Figure 7, right) portrays a more vivid representation of vegetation condition. While EVI values span from 0 to 0.7, the central, northern, and southeastern portions of the study area display consistently higher EVI values compared to the corresponding NDVI map. This indicates a persistence of vegetation structure and canopy integrity in these zones. EVI's improved sensitivity to dense vegetation and its reduced influence from soil background effects likely contribute to this more robust representation of vegetative health.

Notably, the EVI map highlights greener and denser vegetation along river corridors and in pockets scattered across the central region, suggesting areas of intact woodland or localized vegetation recovery. The spatial heterogeneity visible in the EVI composite may reflect variations in land management practices, microclimatic differences, or targeted conservation efforts that have maintained or improved vegetation conditions despite broader landscape pressures.

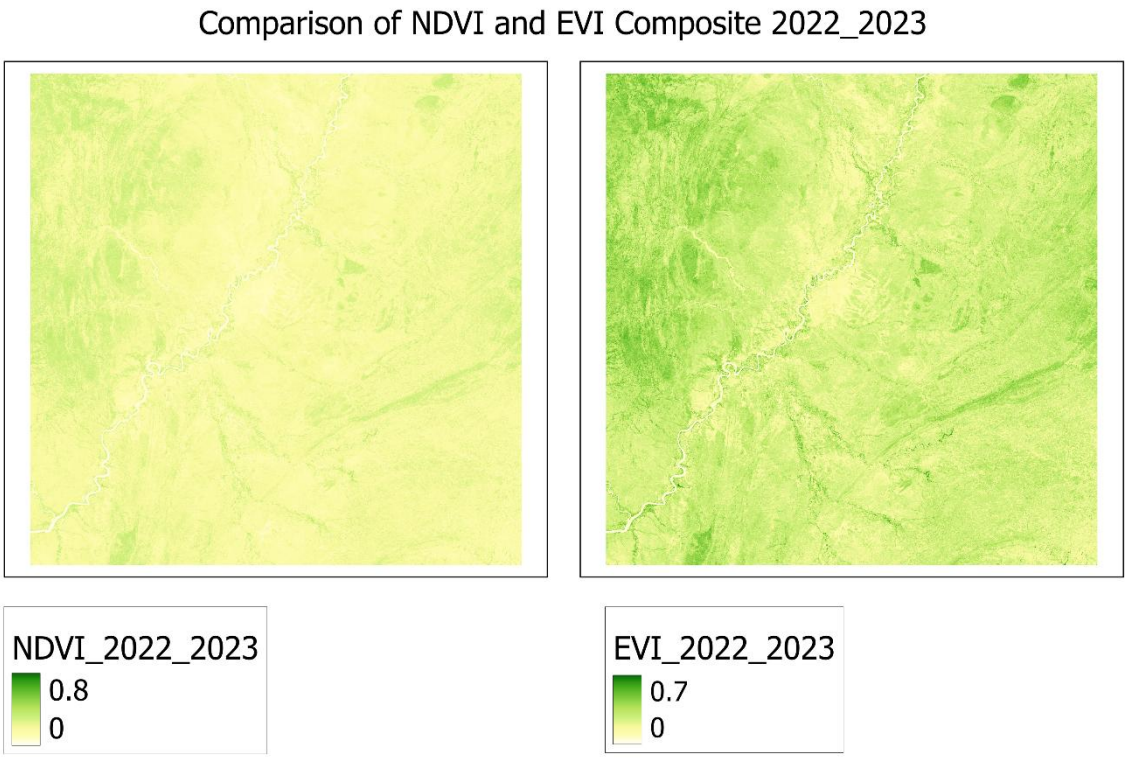

Figure 7: Comparison of NDVI and EVI composite images for the 2022–2023 period

Source: Author's work

4.2 Vegetation Classification Results

The vegetation cover classification based on NDVI and EVI for the two time periods, 2017–2018 and 2022–2023, offers a deeper insight into vegetation's spatial and temporal dynamics in the study area. By categorizing continuous NDVI and EVI values into discrete vegetation classes, namely, Very Low Vegetation, Low Vegetation, Moderate Vegetation, and High Vegetation, the landscape was simplified for comparative analysis and visualization of ecological changes. The classification outputs for both NDVI and EVI indices reveal notable differences and patterns in vegetation distribution and density across the two periods.

4.2.1 Vegetation Classes 2017 – 2018

Figure 8 displays the classified vegetation maps for 2017–2018 derived from NDVI (left) and EVI (right). These maps present a detailed distribution of vegetation cover, segmented into four distinct categories based on thresholds applied to the index values. The NDVI-based classification shows that Moderate to High Vegetation covered a significant portion of the landscape, particularly in the northern and northwestern regions. These areas appear in medium to dark green shades, indicating healthy and dense vegetation, typical of Miombo woodlands. The Low Vegetation and Very Low Vegetation classes were mainly distributed along river corridors and fragmented patches, especially toward the southeast, where anthropogenic activities such as cultivation are more intense. The EVI-based classification supports this pattern but displays higher spatial contrast and vegetation variability. The EVI map emphasizes subtle structural differences in the vegetation canopy, identifying more heterogeneity in moderately vegetated zones. Areas marked as Moderate Vegetation in the EVI map extend more diffusely compared to the NDVI classification, especially around transition zones between wooded and open areas.

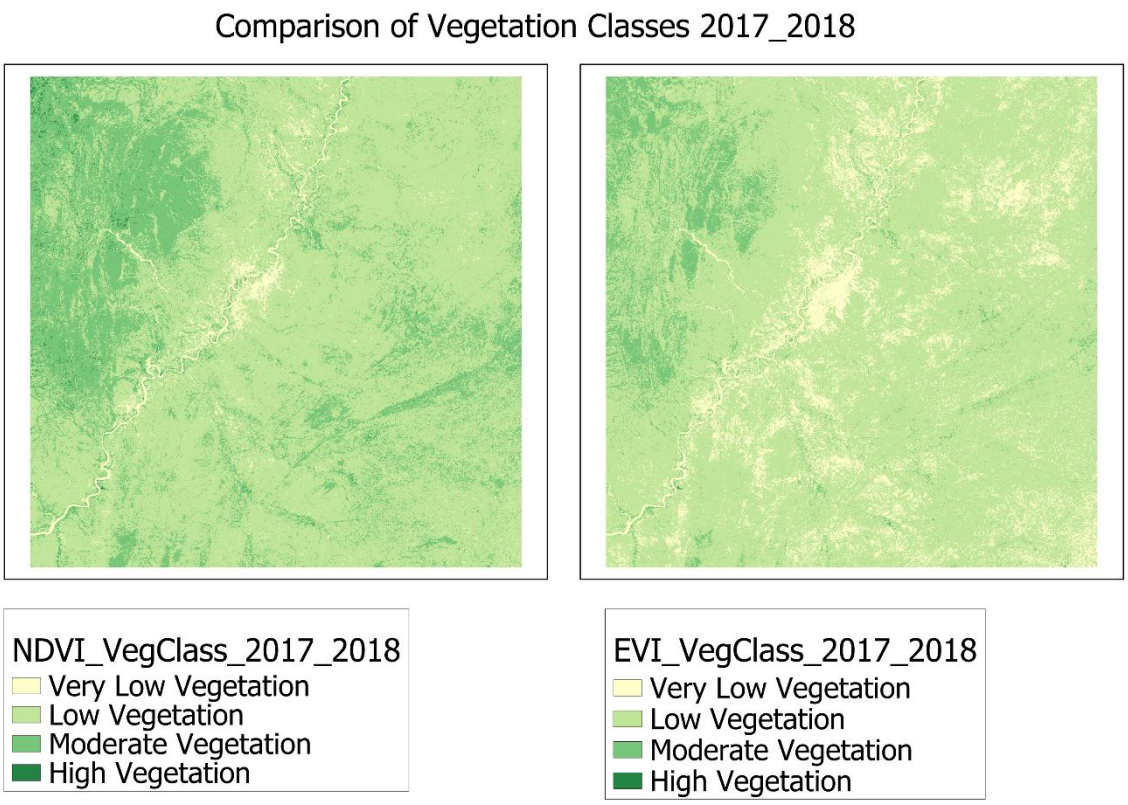

Figure 8: Vegetation Classification Maps for 2017–2018 using NDVI and EVI

Source: Author's own creation

4.2.2 Vegetation Classes 2022 – 2023

Figure 9 presents the classified vegetation maps for the 2022–2023 period, generated from NDVI and EVI indices. These maps categorize the landscape into four vegetation density classes: Very Low Vegetation, Low Vegetation, Moderate Vegetation, and High Vegetation. The outputs provide valuable insights into the spatial structure of vegetation cover and its condition across the study area during the most recent composite period.

In the NDVI-based classification map (Figure 9, left), a notable dominance of Low Vegetation and Very Low Vegetation classes is observed across much of the landscape. Light yellow and pale green tones are widely distributed across the central and northern sectors. This distribution pattern suggests a general decline in vegetation density and health, likely influenced by anthropogenic activities such as agriculture, deforestation, and settlement expansion, combined with potential environmental stressors like prolonged dry spells.

Moderate Vegetation areas are more fragmented than in the previous period and are now primarily located along river corridors and within isolated forest patches. High Vegetation zones, shown in darker green, are minimal, mainly confined to protected areas or regions with minimal human disturbance. This fragmentation of denser vegetation classes underscores increasing pressures on landscape degradation over time.

The EVI-based classification map (Figure 9, right) presents a slightly different and more optimistic picture. While Very Low Vegetation still occupies significant portions of the study area, there is a broader and more continuous distribution of Moderate Vegetation across the southern and central regions compared to the NDVI-derived classification. This indicates that EVI captures more structural integrity within vegetation canopies that NDVI may underestimate due to soil and background influences.

Moreover, the EVI classification reveals sharper contrasts along riparian zones. High Vegetation persists in narrow but continuous strips, reflecting moisture retention and the protective role of riverine ecosystems. These differences highlight EVI's enhanced capability to discriminate vegetation conditions, especially in transitional and high-biomass environments.

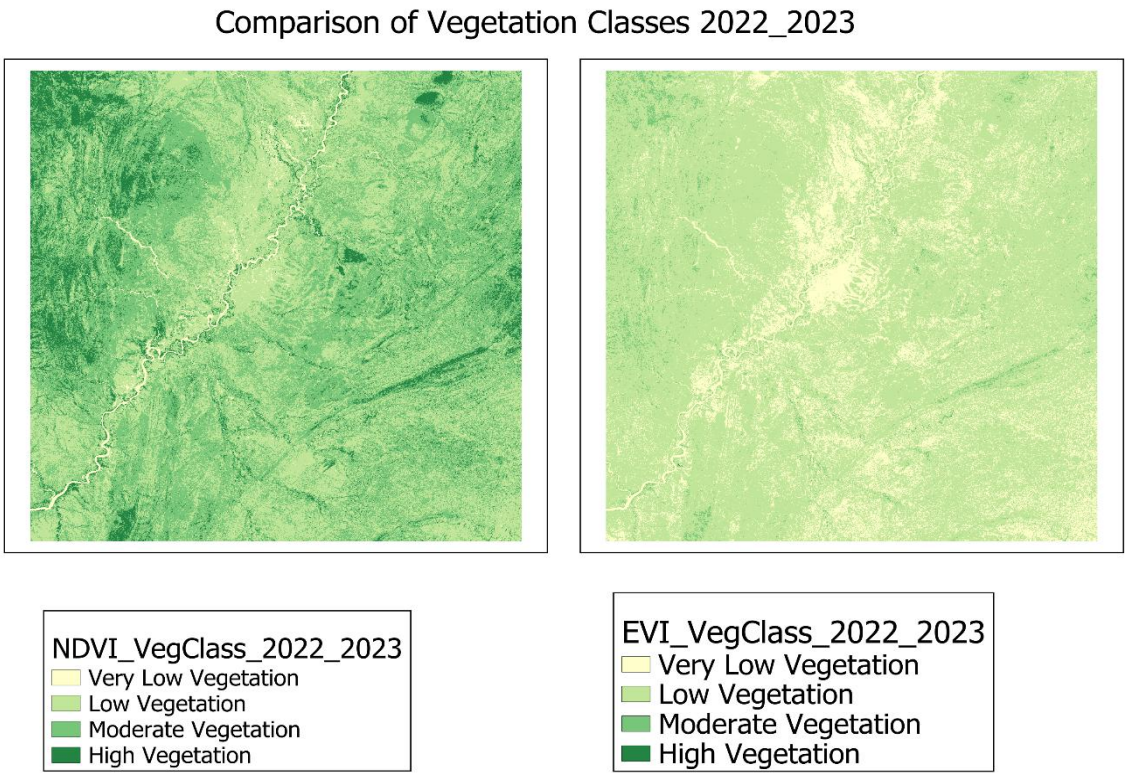

Figure 9: Vegetation Classification Maps for 2022–2023 using NDVI and EVI

Source: Author's work

Table 3: NDVI Vegetation Class Area Summary (2017–2018 vs 2022–2023)

Vegetation Class	**Class Code**	**2017–2018 Area (ha)**	**2022–2023 Area (ha)**
Very Low Vegetation	1	33,907.36	568,978.10
Low Vegetation	2	845,885.10	631,043.60
Moderate Vegetation	3	315,071.50	159,130.90
High Vegetation	4	5,316.89	—

Table 3: NDVI Vegetation Class Area Summary

Source: Author's work

Table 4: EVI Vegetation Class Area Summary (2017–2018 vs 2022–2023)

Vegetation Class	**Class Code**	**2017–2018 Area (ha)**	**2022–2023 Area (ha)**
Very Low Vegetation	1	173,734.20	175,597.10
Low Vegetation	2	92,841.00	921,167.60
Moderate Vegetation	3	101,480.50	103,127.40
High Vegetation	4	125.14	288.80

Table 4: EVI Vegetation Class Area Summary

Source: Author's work

4.3 NDVI and EVI Difference Map Analysis

This section presents an in-depth analysis of the NDVI and EVI difference maps, derived by subtracting the 2017–2018 composite imagery from the 2022–2023 composite imagery. The resulting difference layers provide a spatial representation of vegetation change over the six years, offering insights into degradation patterns, stability, and regrowth within the Miombo woodland ecosystem.

The NDVI difference map in Figure 10 displays values ranging from approximately -1.0 to +0.9. Areas rendered in shades of red signify a decline in vegetation health or cover, while green tones indicate an increase, associated with vegetation recovery or densification. Much of the study area appears light green to yellow, suggesting overall stability or modest improvement in vegetation density. Pockets of pronounced NDVI decline, highlighted in darker red, are mainly located in the landscape's northwestern, western, and southern sectors. These declines may be linked to anthropogenic disturbances such as agricultural expansion, settlement encroachment, fuelwood harvesting, and environmental stressors like extended dry periods. Conversely, areas showing positive NDVI changes, particularly in central and eastern zones, may reflect regrowth, reduced land pressure, or effective conservation measures. However, the NDVI difference histogram in Graph 1 is sharply centered around zero, indicating that most vegetation changes were limited in magnitude and extent.

The EVI difference map, also in Figure 10, presents a different picture, with a dominant red tone suggesting more widespread vegetation loss. Although EVI is typically less affected by soil background noise and more sensitive to structural canopy changes, the difference image shows that large portions of the landscape experienced negative change. Green patches, indicating gains, appear more scattered, especially in the northeastern and central-eastern zones. The EVI histogram in Graph 2 further confirms this trend, showing a narrower and more symmetric curve centered slightly below zero, pointing to general declines in EVI values. This suggests canopy thinning or structural degradation may occur, even in areas where NDVI appears stable or improving.

Overall, the comparison between NDVI and EVI difference maps underscores the importance of using both indices. While NDVI suggests general vegetation stability with limited gains, EVI highlights a more cautious perspective, with subtle declines in vegetation structure. This contrast reflects the unique sensitivity of each index and supports the need for multi-index

approaches when assessing ecological change in dynamic ecosystems like the Miombo woodlands.

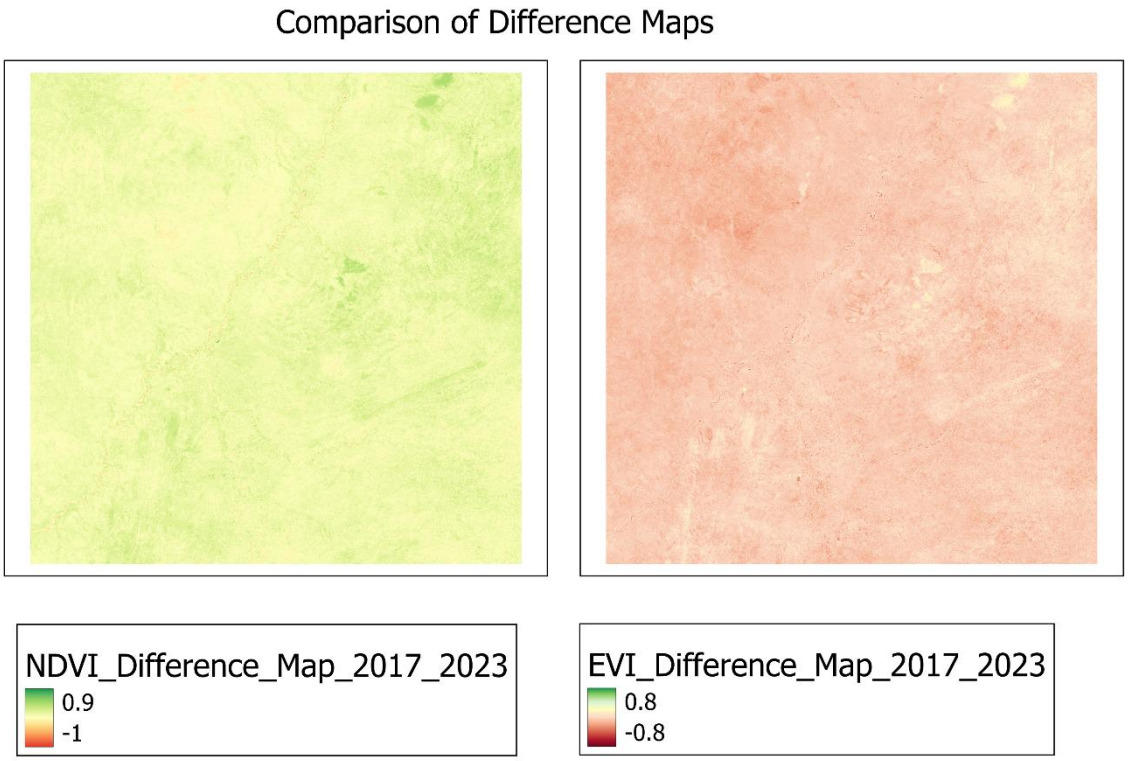

Figure 10: Comparison of NDVI and EVI Difference Maps (2017–2023)

Source: Author's own creation

Graph 1 presents the histogram of NDVI difference values between 2017 and 2023, illustrating the distribution of vegetation change across the study area.

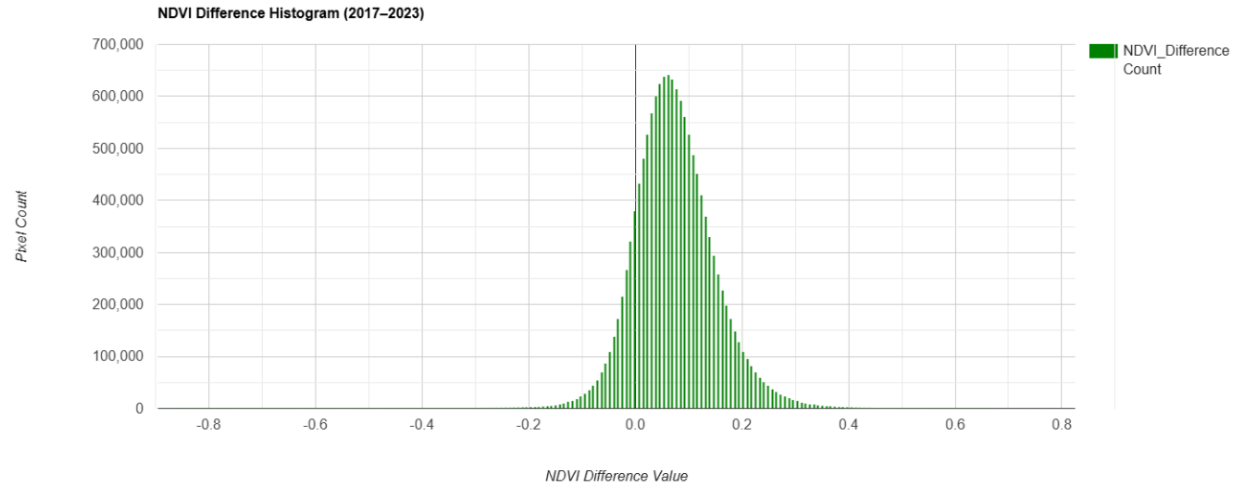

Graph 1:NDVI difference histogram showing vegetation changes between 2017 and 2023

Source:Author created using Google Earth Engine

Graph 2 shows the EVI difference histogram for the 2017–2023 period, highlighting the variation in vegetation structural changes detected using the EVI index.

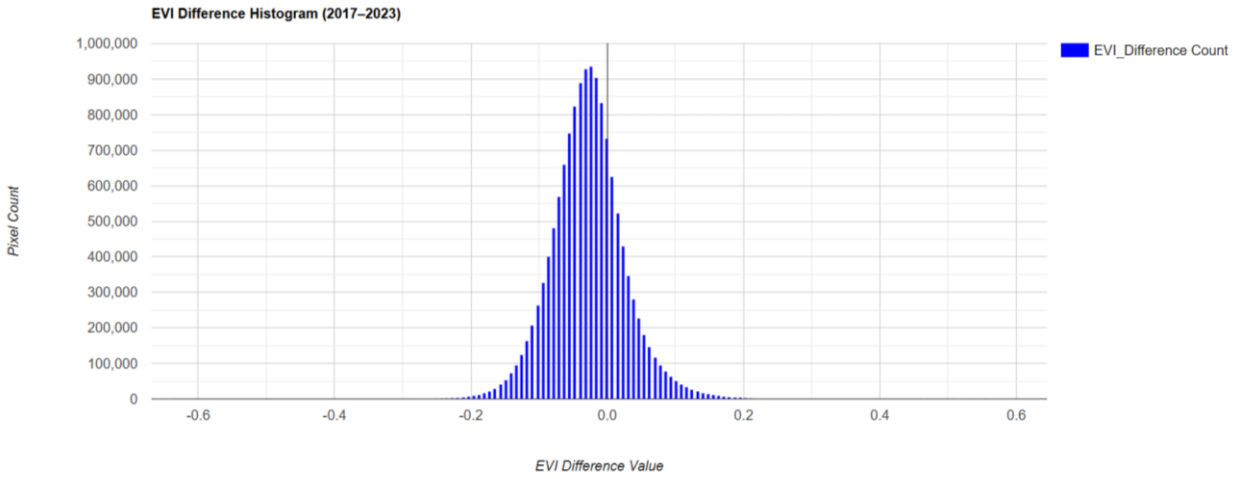

Graph 2: EVI difference histogram illustrating vegetation changes from 2017 to 2023

Source:Author created using Google Earth Engine

4.4 Change Direction Analysis

This section analyzes vegetation change direction across the study area between 2017 and 2023, based on the Normalized Difference Vegetation Index (NDVI) and the Enhanced Vegetation Index (EVI). Change direction maps were generated by categorizing pixel-wise changes into three classes: Increase, Decrease, and No Change, providing crucial insights into the spatial dynamics of vegetation over the six-year period.

The NDVI change direction map (Figure 11, left) reveals a predominant trend of vegetation increase across much of the study area. Green-colored regions, which signify a positive change in NDVI values, dominate the landscape, particularly within the central, eastern, and southern parts. In contrast, indicating vegetation decrease, red regions are more sparsely distributed and mainly concentrated in isolated patches along the northwestern and southwestern zones. Gray areas representing stable or unchanged vegetation conditions are scattered throughout, but occupy a smaller proportion than the areas of increase.

The spatial distribution of green areas suggests localized regrowth or densification of vegetation, possibly linked to land abandonment, conservation measures, or favorable climatic conditions during the latter years of the study period. The relatively limited occurrence of red patches indicates that while some localized degradation occurred, the broader Miombo woodland exhibited resilience and signs of recovery over the timeframe analyzed. These results align well with the NDVI difference histogram, where a slight positive shift was observed.

In contrast, the EVI change direction map (Figure 11, right) portrays a more balanced and heterogeneous pattern of vegetation dynamics. Areas of vegetation decrease (red) are more pronounced and widespread than the NDVI-based map, particularly dominating the northwestern and western regions of the landscape. Meanwhile, vegetation increases (green) areas are less extensive but are distinctly present, mainly clustering in the central-eastern and southeastern parts of the study area. The proportion of gray regions indicating no significant change is notably higher in the EVI change direction map than in the NDVI map, reflecting EVI's greater sensitivity to canopy structure and tendency to register less change in moderately vegetated or dense forest areas.

This comparison underscores the complementary behavior of NDVI and EVI in detecting vegetation change. NDVI tends to highlight broader changes, including sparse vegetation dynamics, while EVI provides a finer detection of changes in denser canopies and more structurally complex vegetation types. Together, the two indices offer a nuanced understanding of the Miombo woodland vegetation dynamics, revealing that while signs of regrowth exist, ongoing localized degradation persists, particularly in areas under anthropogenic pressure.

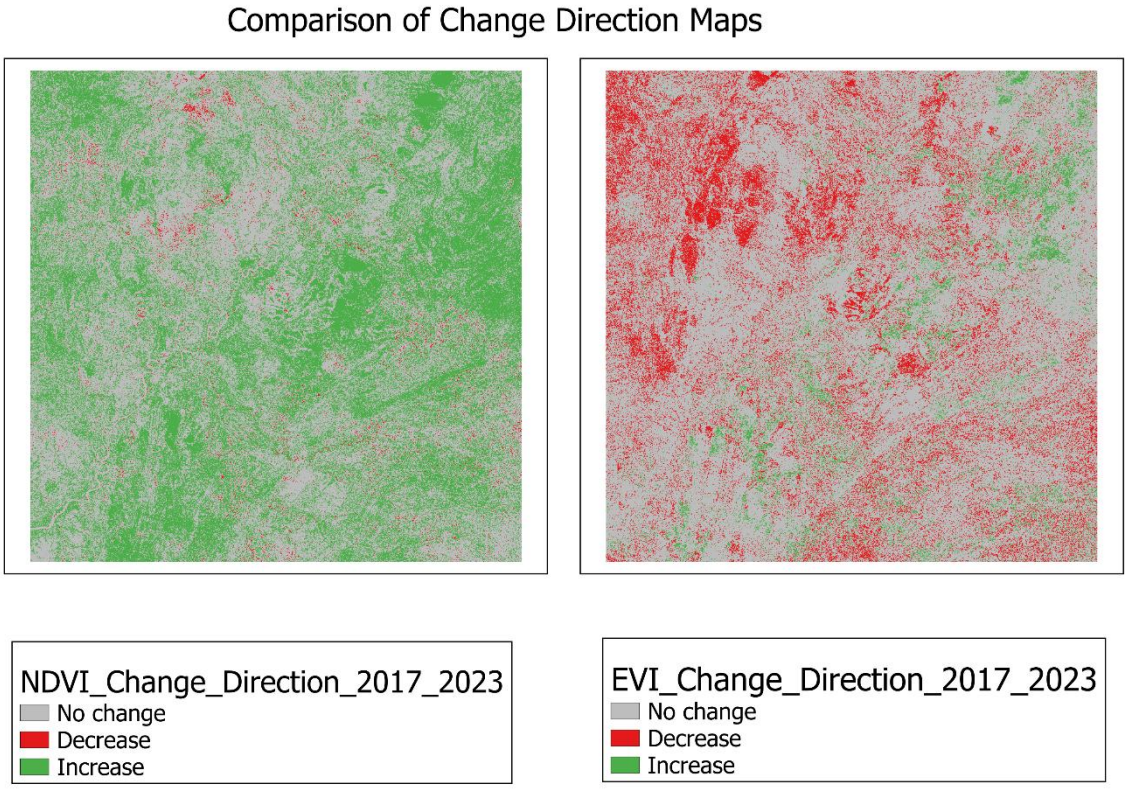

Figure 11: Comparison of Change Direction Maps for NDVI and EVI (2017–2023)

Source: Author's work

4.5 Vegetation Change Map Results

The vegetation change maps derived from NDVI and EVI indices between 2017 and 2023 provide a detailed spatial representation of land cover transitions across the study area. These maps classify the landscape into various transition types, including woodland, bushland, grassland, and bare land conversions, allowing a comparative assessment of vegetation dynamics using two different vegetation indices. The applied classifications are consistent across NDVI- and EVI-based products, facilitating a direct comparison of landscape changes and trends identified through each index.

4.5.1 NDVI and EVI-Based Change Map

The NDVI-based change map (Figure 12, left) reveals a dominant pattern of vegetation degradation over the six-year period. Transitions such as Woodland to Bushland and Woodland to Grassland, highlighted in orange and yellow hues, are widely distributed across the study region, particularly prevalent in the western and central zones. These transitions suggest a progressive thinning of vegetation cover, likely driven by anthropogenic activities such as agricultural encroachment, selective logging, and settlement expansion. The Woodland to Woodland class, shown in gray, still occupies substantial portions of the landscape, indicating areas of vegetation stability. However, compared to positive transitions, degradation patterns are visually more extensive. Bare land transitions, especially Bare to Grassland and Bare to Bushland, are less common but present in isolated pockets, suggesting areas of limited regrowth following disturbance or abandonment.

In contrast, the EVI-based change map (Figure 12, right) presents a more balanced depiction of vegetation dynamics. While Woodland to Woodland remains a prominent class, there is a greater distribution of positive transitions, notably Grassland to Woodland and Bushland to Woodland, shown in shades of green. These patterns are especially concentrated in the northeastern and southeastern parts of the study area, indicating localized zones of vegetation recovery and canopy densification.

Unlike the NDVI map, the EVI change map shows fewer extreme degradation transitions and a higher proportion of vegetation stability and gain. The visibility of classes such as Grassland to Grassland and Bushland to Bushland indicates structural maintenance of existing vegetation types rather than complete shifts to bare or degraded categories. This distinction underscores the sensitivity of EVI to subtle changes in vegetation structure and canopy density.

4.5.3 Comparative Analysis

A comparative evaluation of the updated NDVI and EVI change maps provides a clearer and more nuanced understanding of vegetation dynamics across the study area between 2017 and 2023. The NDVI change map highlights broad-scale degradation trends, especially transitions from woodland to sparser classes like bushland and grassland. Large portions of the western

and southwestern regions display significant degradation (in red), consistent with anthropogenic land pressure such as deforestation, charcoal production, and shifting cultivation.

The EVI change map, in contrast, reveals more localized vegetation improvements (green patches), particularly in the northeast and along riparian zones. These gains represent structural improvements in canopy density that may not be as easily captured by NDVI due to its sensitivity to background noise and saturation effects in denser vegetation.

This divergence illustrates the complementary nature of the two indices. NDVI is useful for identifying broad spatial trends and general vegetation loss, while EVI excels at detecting subtle regrowth and structural enhancements in vegetation. The combined use of both indices enables a more balanced interpretation of ecological change — revealing both degradation hotspots and areas of recovery or stabilization. These results reinforce the importance of multi-index approaches for assessing complex woodland ecosystems such as the Miombo biome.

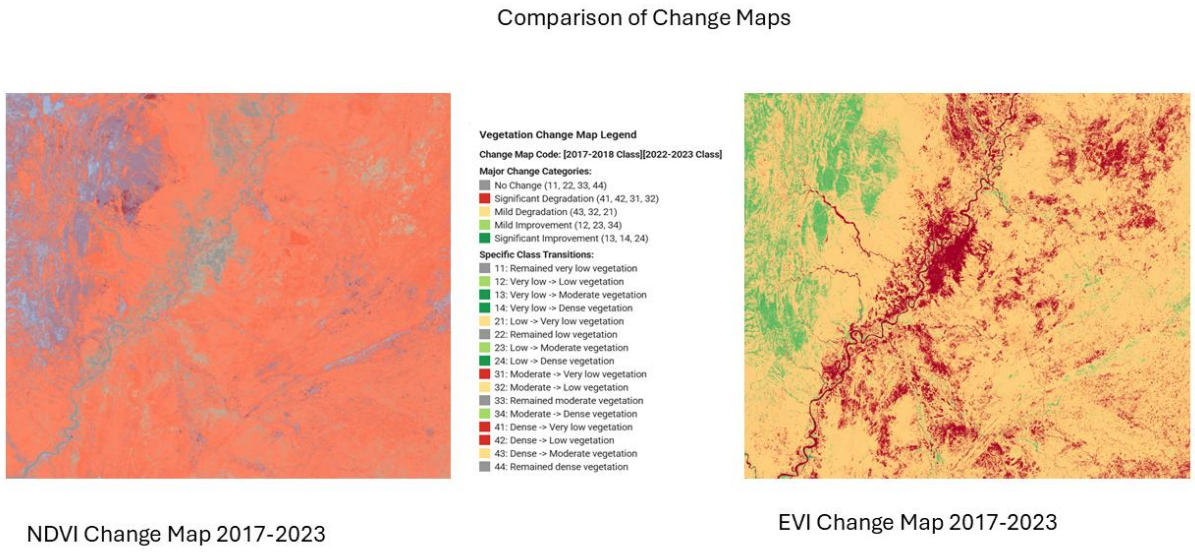

Figure 12: Comparison of Change Maps for NDVI and EVI (2017–2023)

Source: Author's work

Table 5 shows Random Forest-based vegetation change detection statistical summary.

Change Direction	Area (ha)	Source
No Change	67993	NDVI
Decrease	24477	NDVI
Increase	534828	NDVI
No Change	929381	EVI
Decrease	237382	EVI
Increase	72466	EVI

Table 5: NDVI and EVI Transition areas

Source: Author's work

The NDVI and EVI summaries reveal contrasting patterns of vegetation change. NDVI indicates widespread stability with moderate improvement and limited decline, while EVI shows more extensive structural degradation and fewer gains. This highlights NDVI's sensitivity to overall greenness and EVI's ability to detect finer-scale vegetation structure loss.

4.6 Random Forest-Based Change Detection Results

This section presents the results of vegetation change detection using a supervised classification approach based on the Random Forest (RF) algorithm. Unlike the threshold-based NDVI and EVI classifications, which relied on predefined index thresholds, the RF method applies a data-driven approach trained on stratified sample points derived from classified imagery. By incorporating both spectral bands and vegetation indices, the RF model captures more complex patterns of vegetation structure and change across the Miombo woodland landscape.

The RF-based classification outputs offer a complementary perspective to the threshold results, providing enhanced insight into the spatial distribution of vegetation change dynamics over the six-year study period. In addition to the NDVI and EVI difference-based analyses, a change map was generated from the Random Forest (RF) classification outputs for 2017–2018 and 2022–2023 (Figure 13). The RF change map categorizes vegetation transitions into five main

types, including both degradation and improvement. Visually, it aligns closely with the NDVI-based results, showing widespread degradation in the western and southwestern regions. However, it also captures smaller pockets of improvement in the central and northeastern zones, consistent with the EVI findings. This reinforces the utility of Random Forest in capturing complex land cover dynamics in Miombo ecosystems.

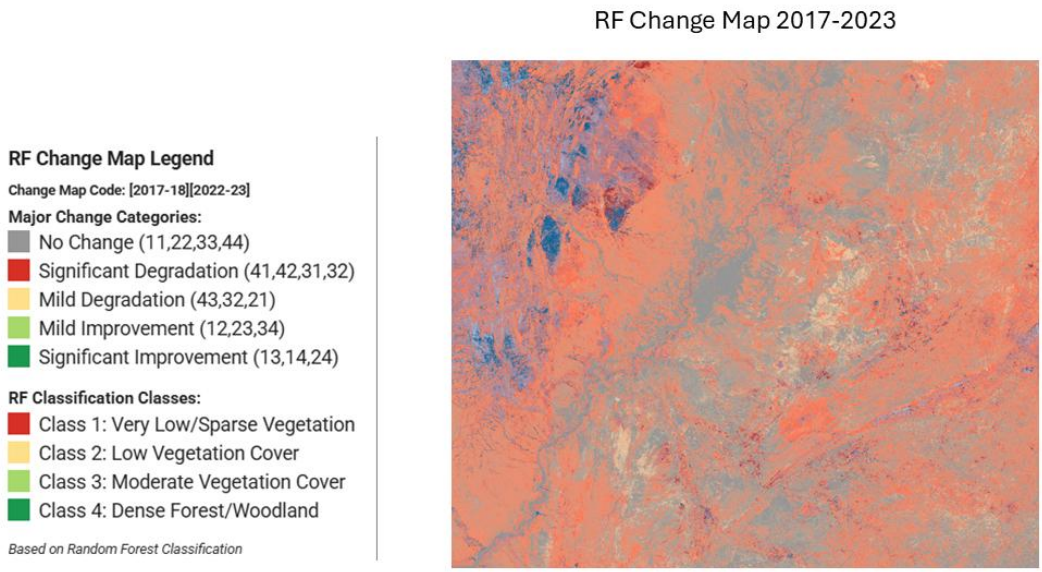

Figure 13: Random Forest-Based Change Map 2017–2023

Source: Author's work

4.6.1 RF Classification and Change Direction Mapping

The RF classifier was trained on a carefully curated dataset of 100 vegetation training points labeled across four vegetation classes: Very Low, Low, Moderate, and High. This training set, derived from high-resolution Google Earth imagery, was used to classify Sentinel-2 composite imagery for 2017–2018 and 2022–2023. The classification used spectral bands (B2, B3, B4, B8) and vegetation indices (NDVI, EVI, SAVI) to improve model learning.

Post-classification, the change direction was derived by comparing the two classified layers. The output was grouped into three categories:

- **No Change:** where vegetation class remained the same
- **Increase:** where vegetation class increased (e.g., from Low to Moderate)

- **Decrease:** where vegetation class declined (e.g., from Moderate to Low)

Figure 13 illustrates areas of No Change, shown in gray. These regions are relatively dispersed and indicate pockets of stable vegetation conditions. Figure 14 presents zones of Vegetation Decrease in red. Declines are concentrated in the western and southern portions of the study area, likely driven by anthropogenic activities such as agriculture or deforestation. Figure 15 displays areas of Vegetation Increase in green. This includes central and eastern zones, suggesting regrowth or afforestation efforts. Together, these maps provide a comprehensive spatial narrative of vegetative transitions over the six-year period.

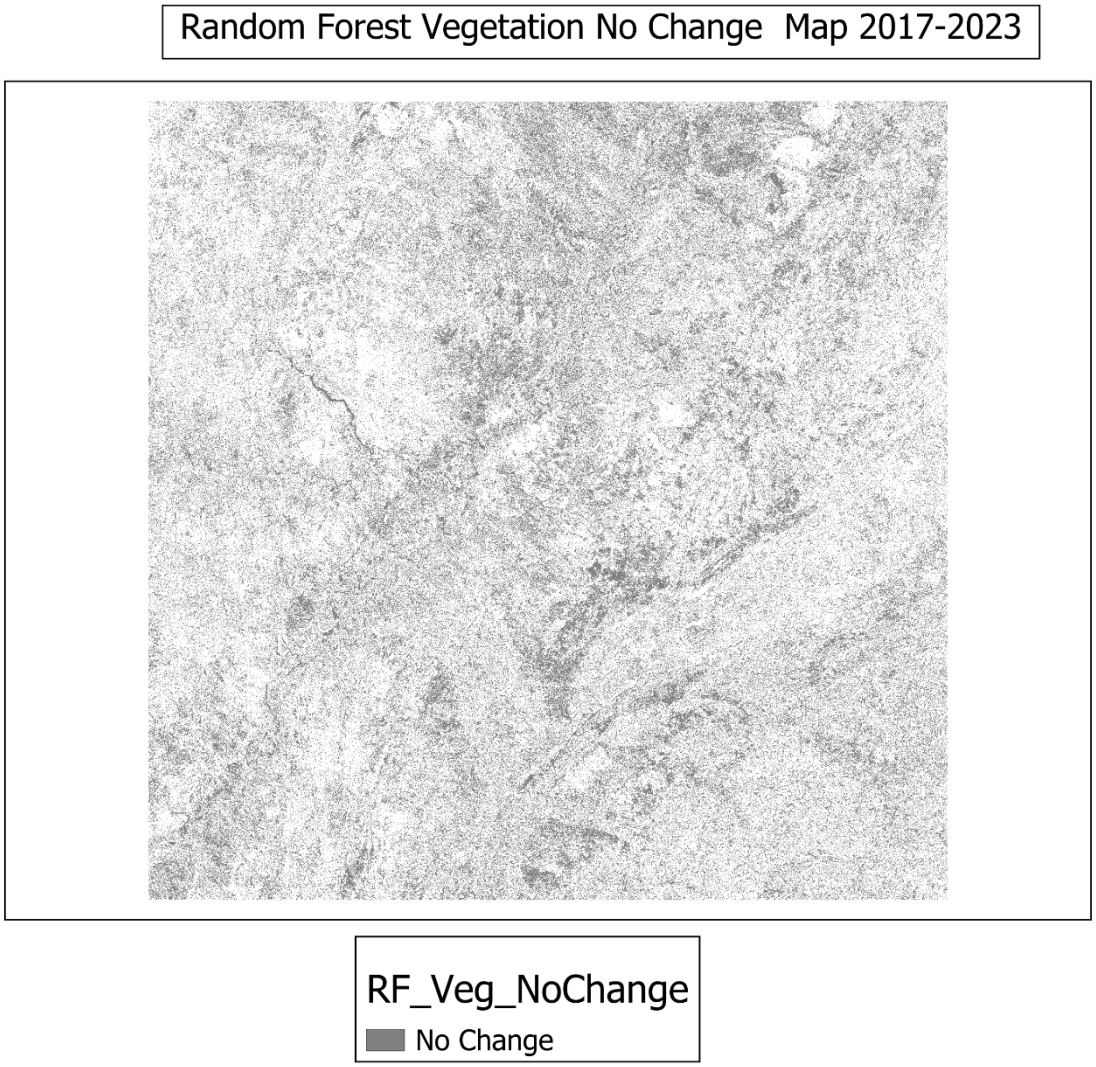

Figure 14: Random forest no change map

Source: Author's work

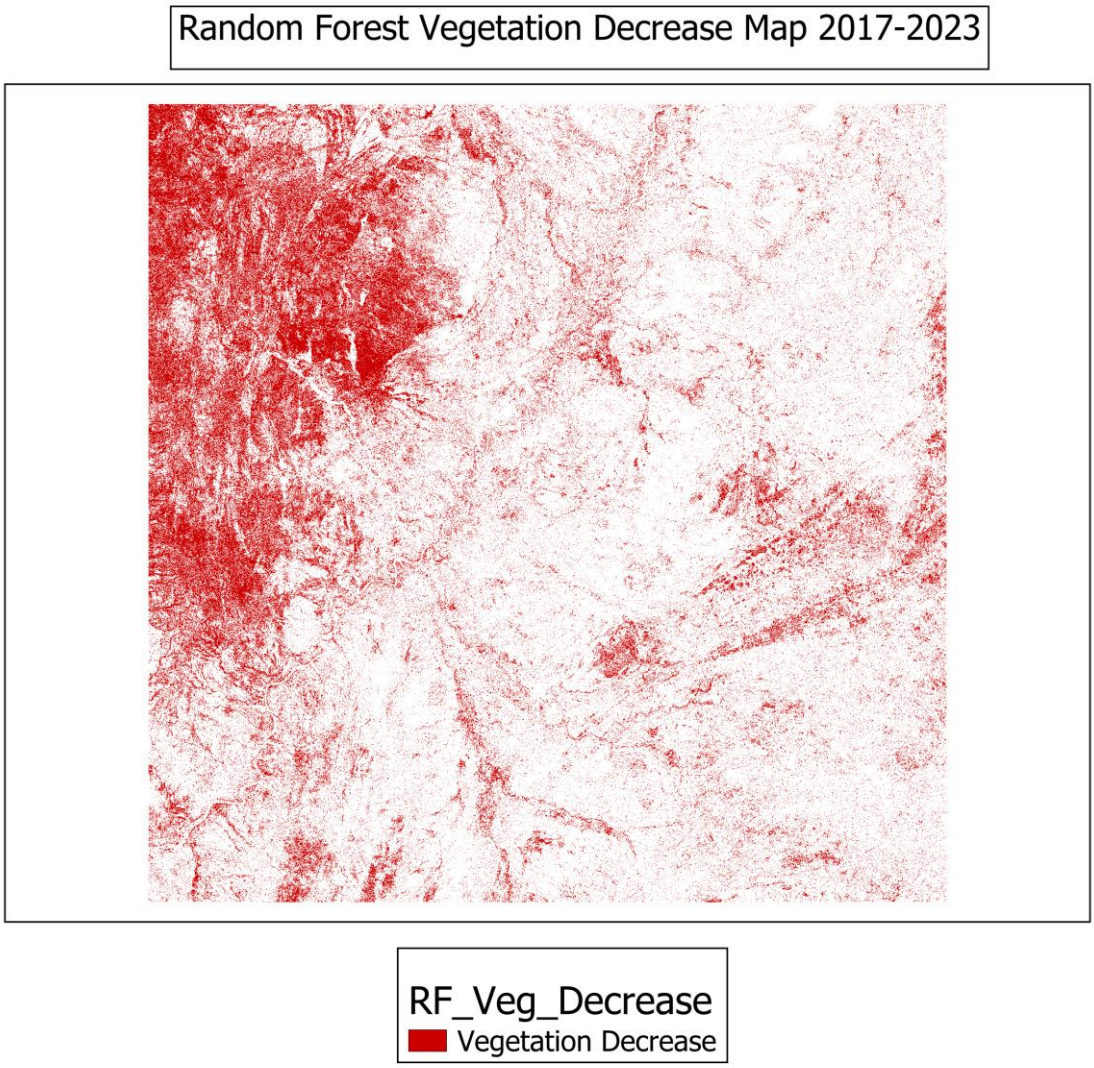

Figure 15:Random forest decrease map

Source: Author's work

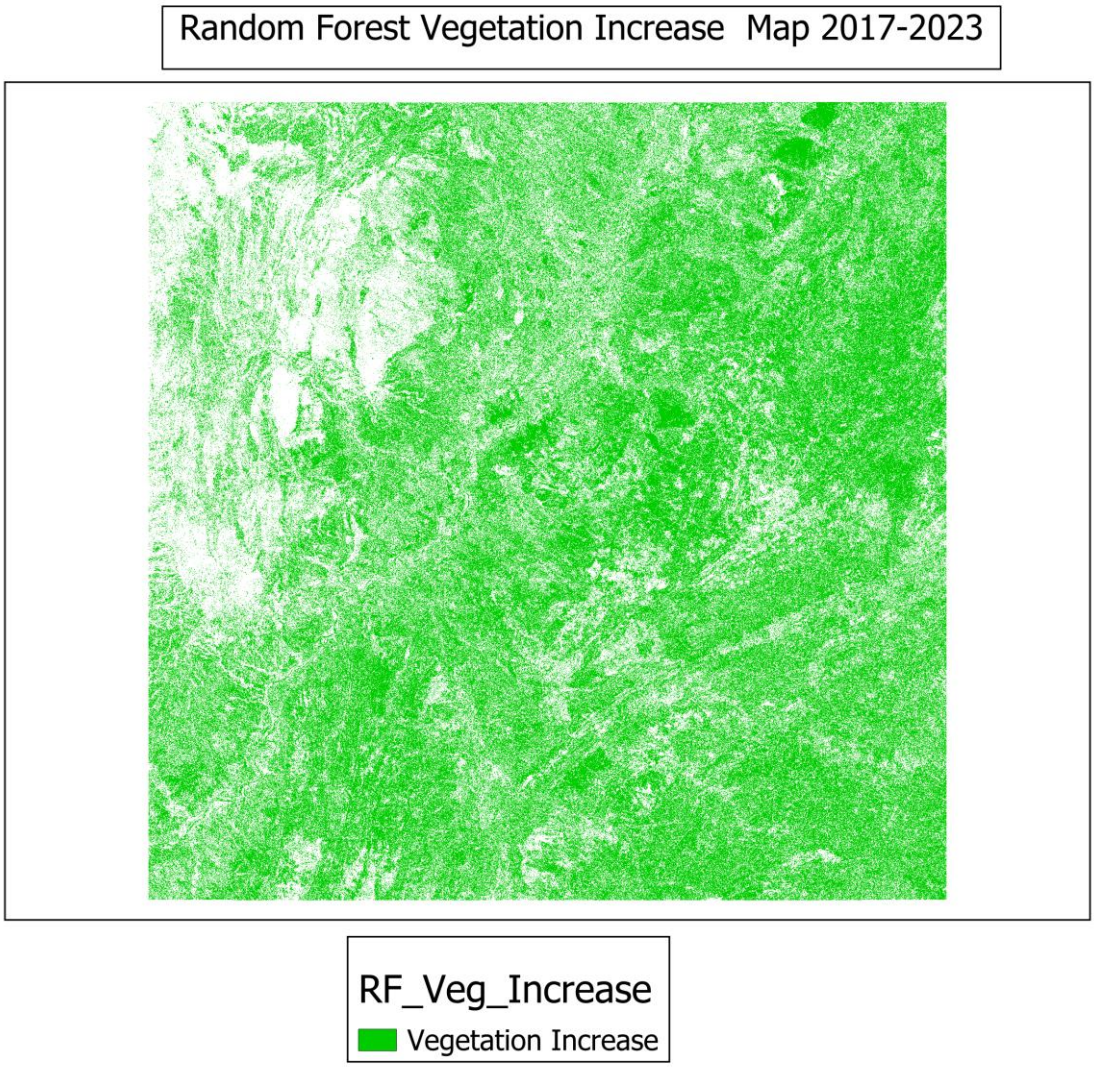

Figure 16:Random forest Increase map

Source: Author's work

4.6.2 Quantitative Summary of RF Transitions

Table 5 shows Random Forest-based vegetation change detection statistical summary. The transition areas were aggregated into three categories:

Change Direction	**Area (ha)**
No Change	**28,567**
Decrease	**16,210**
Increase	**25,104**

Table 6: Random Forest Transition areas

Source: Author's work

The largest portion of the study area remained unchanged 28,567 ha. A significant portion, 25,104 ha, experienced positive vegetation change. Roughly 16,210 ha underwent degradation. These figures underscore that while substantial degradation is evident, regrowth and afforestation appear to have occurred at scale.

4.6.3 Interpretation and Implications

Compared to the earlier NDVI- and EVI-based threshold classification methods, the Random Forest (RF) classification captures more heterogeneous patterns of change, better reflecting field-like variability due to the incorporation of richer features, including NDVI, EVI, SAVI, and Sentinel-2 spectral bands (B2, B3, B4, B8). The RF classifier demonstrates a more detailed and spatially nuanced depiction of vegetation dynamics across the Miombo woodland landscape. The vegetation decrease zones correspond closely with known areas of anthropogenic pressure, particularly in the western and southwestern parts of the study area. These pressures likely stem from agricultural expansion, settlement growth, and deforestation. Conversely, zones showing vegetation increase, particularly in central and eastern corridors, suggest natural regeneration, land abandonment, or successful afforestation efforts.

While the external validation based on an independent 80/20 split yielded a moderate overall accuracy of 50% and a Kappa coefficient of 0.238, an additional internal stratified sample validation demonstrated perfect classification performance, with 100% overall accuracy and a Kappa coefficient of 1.0. The internal assessment reflects a high degree of internal model consistency, whereas the external validation underscores the challenges of generalizing across heterogeneous and spectrally overlapping vegetation types in the Miombo woodland ecosystem.

Together, the RF classification and change analysis provide a more robust and credible depiction of vegetation changes over the six years compared to simpler threshold methods, highlighting both the areas of significant vegetation decline and patches of recovery across the landscape. Figure 16 shows the random forest vegetation classification for both time periods.

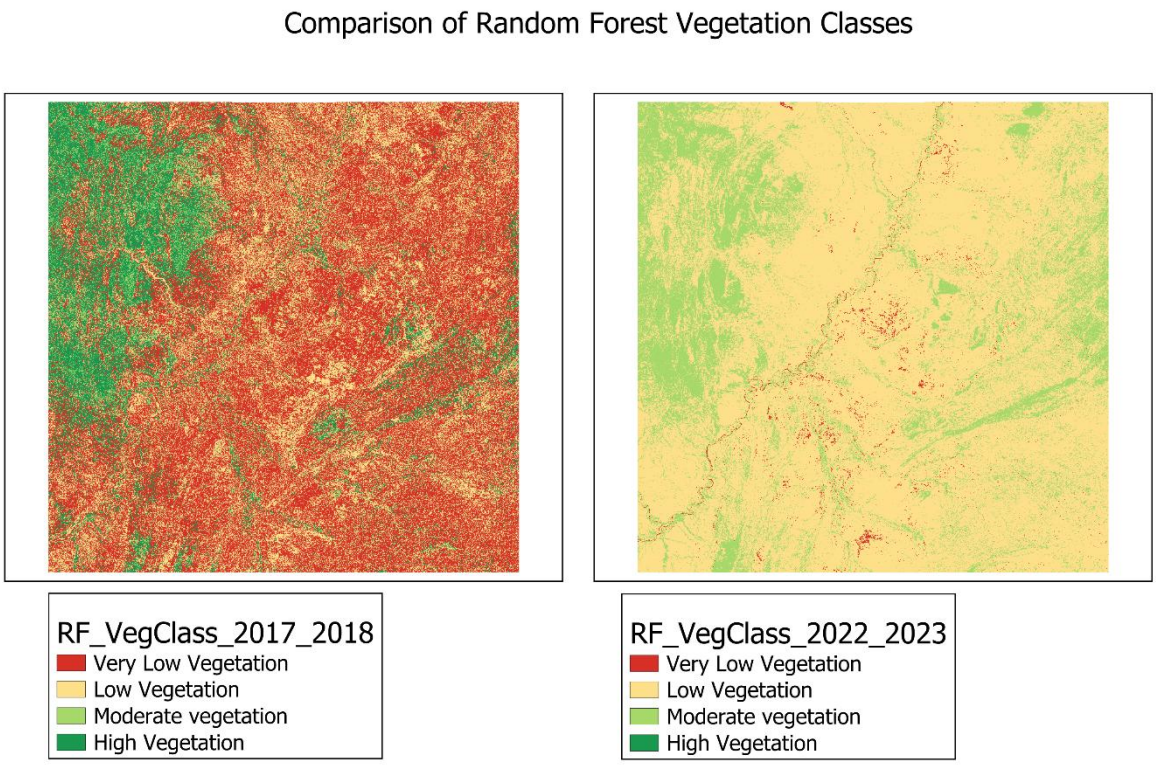

Figure 17: Comparison of Random forest Vegetation classes

Source: Author's work

4.7 Classification Accuracy Assessment

To assess the accuracy of the vegetation classifications produced in this study, threshold-based and Random Forest (RF) supervised classifications were evaluated using ground truth points collected from high-resolution Google Earth imagery. Confusion matrices, overall accuracy, and Kappa coefficients were generated to measure the classification reliability. This section presents the detailed validation results, highlighting the differences between the simpler threshold approach and the machine learning-based RF classification method.

4.7.1 Threshold-Based NDVI and EVI Classification

The threshold-based classification assigned vegetation classes according to fixed NDVI and EVI value ranges. While simple to implement, this method showed limited accuracy when evaluated against **180** manually interpreted ground truth points, collected through visual inspection of high-resolution imagery in Google Earth Pro.

The confusion matrix for NDVI classification (Table 5) revealed substantial misclassification between adjacent vegetation classes, particularly between Very Low (Class 1), Low (Class 2), and Moderate (Class 3) vegetation. These errors reflect the spectral similarity between transitional vegetation zones in Miombo woodlands. The most common confusions occurred between Class 1 and Class 2, and between Class 2 and Class 3.

Actual Class	**Predicted 1**	**Predicted 2**	**Predicted 3**	**Predicted 4**
1	0	4	43	3
2	0	0	38	12
3	1	0	4	26
4	0	0	2	13

Table 7: Confusion Matrix of NDVI classification

Source: Author's work

Overall Accuracy: 46.1%

Kappa Coefficient: 0.28

The Kappa value of 0.2755 indicates only fair agreement between the NDVI classification and the manually interpreted ground truth. This suggests that fixed NDVI thresholds may be insufficient for reliably distinguishing vegetation in mixed woodland environments, where classes tend to overlap spectrally and structurally.

Table 6 shows the EVI confusion matrix based on the same set of 180 validation points. The EVI classification showed a strong bias toward Moderate Vegetation (Class 3), with the majority of samples across all classes misclassified into this single category.

Actual Class	**Predicted 1**	**Predicted 2**	**Predicted 3**	**Predicted 4**
1	0	18	32	0
2	0	2	43	5
3	0	0	15	25
4	0	1	2	19

Table 8: Confusion Matrix of EVI classification

Source: Author's work

Overall Accuracy: 52.2%

Kappa Coefficient: 0.35

The EVI classification performed better than NDVI, achieving 52.2% overall accuracy and a Kappa coefficient of 0.3485. However, substantial misclassification still occurred, particularly with a strong bias toward Moderate Vegetation (Class 3), likely due to EVI's sensitivity to canopy density and soil reflectance.

4.7.2 Random Forest (RF) Classification Accuracy

A Random Forest (RF) machine learning model was applied to improve the classification performance. RF learns from the data instead of using fixed thresholds and is capable of handling more complex relationships between spectral bands and vegetation classes.

The ground truth dataset of 180 manually interpreted points was randomly split into 60% for training (112 points) and 40% for validation (68 points). The model was trained using Sentinel-2 spectral bands (B2, B3, B4, B8) and evaluated using the held-out validation set.

Table 7 presents the confusion matrix for the RF classifier. Unlike the threshold-based methods, RF achieved higher accuracy across all classes, with better separation between vegetation types.

Actual Class	**Predicted 1**	**Predicted 2**	**Predicted 3**	**Predicted 4**
Class 1	0	15	5	0
Class 2	0	3	10	0
Class 3	0	1	14	6
Class 4	0	0	1	10

Table 9: Randon Forest Confusion Matrix

Source: Author's work

Overall Accuracy: 61.8%

Kappa Coefficient: 0.48

The Kappa value of 0.4819 indicates moderate agreement between RF predictions and ground truth, demonstrating improved consistency over the threshold-based methods. RF could better distinguish overlapping vegetation classes by learning from spectral patterns, particularly when NDVI and EVI were used as additional input features. Graph 3 below shows the classification accuracy and kappa coefficient in a chart.

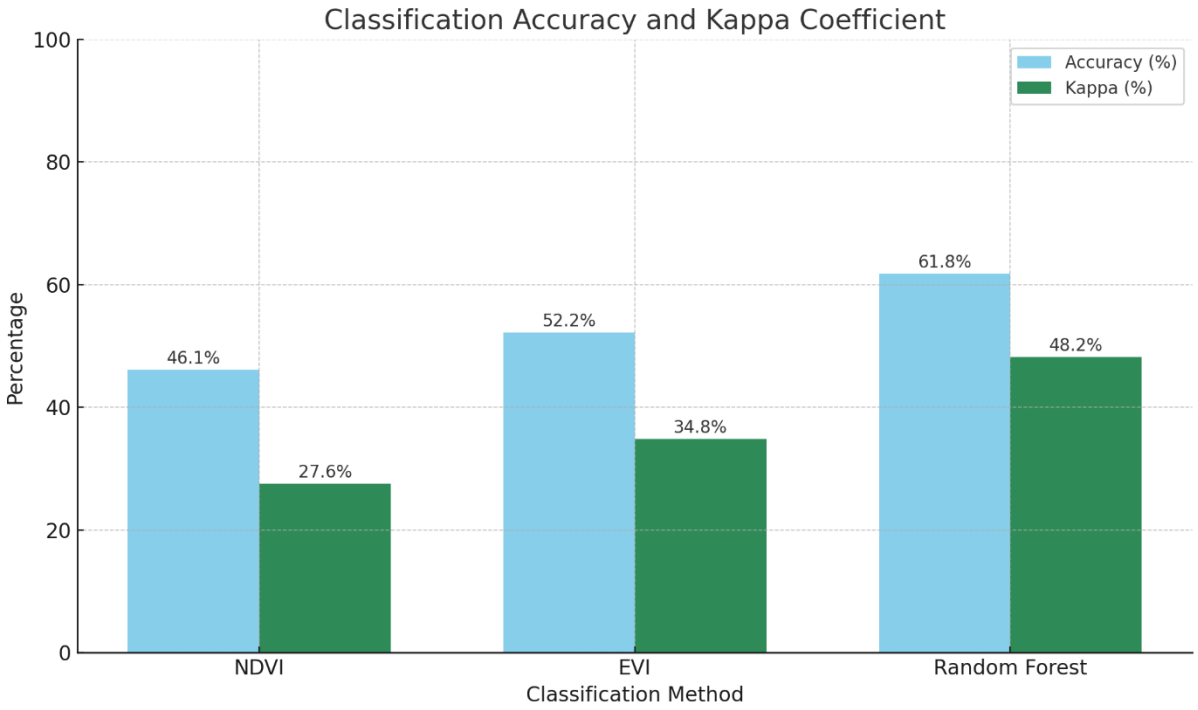

Graph 3: Accuracy Assessment of Threshold-Based and Random Forest Classifications

Source: Author's work

The classification results reveal a clear performance gap between threshold-based and machine learning approaches. While NDVI and EVI methods achieved 46.1% and 52.2% accuracy, respectively, both demonstrated limited agreement with the ground truth data, largely due to spectral confusion between adjacent vegetation classes. In contrast, the Random Forest model significantly outperformed the threshold-based methods, achieving a higher accuracy of 61.8% and a Kappa coefficient of 0.48, indicating moderate agreement. These findings underscore the limitations of fixed index thresholds in complex ecosystems like Miombo woodlands and reinforce the value of data-driven approaches for more accurate vegetation classification.

5. Discussion

This study investigated spatial and temporal vegetation dynamics within the Miombo woodland ecosystem using Sentinel-2 imagery, leveraging both threshold-based and Random Forest (RF) supervised classification approaches. The results highlighted notable patterns of vegetation stability, degradation, and localized regeneration over the six years between 2017 and 2023. Threshold-based classifications provided a broad overview of vegetation class transitions, while the RF classification offered a more detailed and data-driven perspective, capturing subtler shifts across the landscape.

The observed trends align with broader patterns reported in Miombo woodland studies across southern Africa, where anthropogenic pressures such as agricultural expansion, deforestation, and settlement growth are key drivers of vegetation decline. At the same time, areas under protection or natural regeneration exhibit stability or improvement. The comparison between NDVI- and EVI-derived results further emphasized the importance of using multiple indices to interpret vegetation structure and change accurately.

The observed classification accuracies highlight the limitations of simple thresholding in complex woodland environments and the advantages offered by supervised machine learning approaches like Random Forest.

In the following sections, the implications of these findings are explored regarding regional land use patterns, ecological resilience, and the methodological strengths and limitations of the applied classification techniques. Recommendations for conservation efforts and future remote sensing applications in woodland ecosystems are also discussed.

5.1 Vegetation Index Composites

The NDVI and EVI composites generated for the two time periods revealed consistent spatial patterns of vegetative greenness, albeit with clear differences in sensitivity and contrast. NDVI composites generally presented smoother gradients of vegetation cover across the landscape, while EVI composites showed more localized distinctions, particularly in areas of denser vegetation and along riparian corridors. The higher sensitivity of EVI to canopy structure, soil background, and atmospheric conditions likely contributed to these variations. This contrast underpins the importance of using both indices for multi-dimensional vegetation analysis.

5.2 Vegetation Change Patterns in the Miombo Woodland

The NDVI and EVI difference maps indicated that much of the study area experienced minor to moderate vegetation change between 2017 and 2023. Histograms for both indices showed distributions centered around zero, with NDVI showing slightly broader variability. Threshold-based change direction maps revealed areas of vegetation decrease, particularly in the western and northwestern zones, but overall stability and gains dominated the central and eastern regions.

The Random Forest classification further refined these observations. Change direction maps generated from RF outputs identified clear vegetation degradation and improvement areas, revealing a finer mosaic of land cover transitions than the threshold methods. Quantitative summaries showed that while a substantial portion of the landscape remained unchanged, notable areas exhibited both densification and degradation, reflecting dynamic land use and ecological processes.

5.3 Drivers of Vegetation Change

Vegetation loss patterns in this study align with known drivers such as agricultural expansion, charcoal production, deforestation, and urban growth. The western and southwestern zones showed the most degradation, likely linked to expanding rural settlements. Conversely, zones of vegetation recovery along rivers and isolated central patches suggest localized natural regeneration, conservation efforts, or reduced land pressure. Microclimatic variability, such as rainfall patterns, may have contributed to these localized gains.

5.4 Comparison of Classification Approaches

The threshold-based classification approach showed moderate performance. For NDVI, the classification achieved an overall accuracy of 46.1% and a Kappa coefficient of 0.28, indicating only fair agreement with ground truth data. For EVI, accuracy improved slightly to 52.2% with a Kappa of 0.35, though misclassifications remained high, especially a strong tendency to overclassify into the Moderate Vegetation class (Class 3).

In contrast, the Random Forest (RF) classifier provided substantially better results. Using a 60/40 training-validation split, the RF model achieved an overall accuracy of 61.8% and a Kappa coefficient of 0.48. This moderate level of agreement reflects an improved ability to

distinguish between overlapping vegetation classes by incorporating multiple spectral features (B2, B3, B4, B8). The model also benefited from the additional inclusion of vegetation indices (NDVI and EVI) in its classification, capturing more subtle structural variations.

These results confirm that machine learning-based classification offers a more robust solution for mapping complex and heterogeneous vegetation environments such as the Miombo woodland, especially when compared to static threshold rules that often fail to capture spectral variability.

5.5 Ecological Implications

Areas of vegetation loss point to ongoing risks to ecosystem services like carbon storage, biodiversity, and water regulation. If degradation continues, woodland fragmentation and reduced resilience are likely. Areas of vegetation recovery offer opportunities for restoration. Natural regeneration, reforestation, and sustainable land management practices can strengthen ecosystem health and support rural livelihoods. Integrated conservation and development strategies are needed to balance land use with woodland conservation.

5.6 Methodological Considerations

Combining Sentinel-2 imagery, vegetation indices, and machine learning provided a robust monitoring framework. Threshold classification offered simplicity, while Random Forest added precision. However, the lack of extensive field-based ground truthing limited the strength of the external validation.

One important consideration in interpreting the vegetation indices (VI) results from this study is the use of Sentinel-2 data products processed with different baselines: Level-1C (L1C) data for 2017–2018 and Level-2A (L2A) data for 2022–2023. The L1C products, which lack atmospheric correction, inherently introduce variations in VI values caused by atmospheric conditions such as aerosol and water vapor content (Drusch et al., 2012; Springer et al., 2017). In contrast, L2A products, atmospherically corrected using ESA's SEN2COR processor, provide more stable and consistent reflectance values suitable for quantitative VI analysis (*S2 Processing*, 2025).

Mixing these processing levels may affect the stability and absolute values of vegetation indices. Although distinguishing general vegetation versus non-vegetation classes is less influenced, quantitative analyses comparing VI values or evaluating more refined vegetation classes could be impacted significantly (Springer et al., 2017). Due to time constraints, consistent atmospheric correction across all datasets could not be performed. Future research should ideally use uniform processing baselines, applying atmospheric corrections such as those provided by SEN2COR or alternative methods like Dark Object Subtraction (DOS) to older datasets to enhance comparability and reliability of quantitative analyses (Valdivieso-Ros et al., 2021).

5.7 Recommendations

This study investigated vegetation change dynamics across the Miombo woodland ecosystem using Sentinel-2 imagery and a combination of threshold-based and Random Forest (RF) supervised classification methods. Based on the findings, this chapter proposes a series of recommendations to inform sustainable land management practices, improve remote sensing methodologies, guide future research, and strengthen policy frameworks for woodland conservation. These recommendations are organized into four main areas:

- Land management and conservation interventions: The study identified several areas, particularly in the western and southwestern parts of the landscape, that experienced significant vegetation decline between 2017 and 2023. These degradation hotspots should be prioritized for targeted restoration initiatives. Land degradation in Miombo woodlands reduces biodiversity and ecosystem services and exacerbates climate vulnerability. Restoration strategies should include natural regeneration support, reforestation with native species, and soil stabilization techniques. Community engagement is critical: restoration projects should involve local stakeholders through participatory planning, offering incentives for stewardship and long-term management. Payment for Ecosystem Services (PES) schemes and community forestry programs could be explored as mechanisms to promote local involvement.

- Promote Sustainable Land-Use and Agroforestry Practices: Land-use pressure remains a key driver of vegetation degradation in Miombo ecosystems. Promoting sustainable agriculture, agroforestry systems, and climate-smart farming practices can help balance food security needs with conservation objectives. Training programs targeting smallholder farmers should emphasize conservation agriculture, minimum tillage, intercropping, and the integration of trees into farming systems. Agroforestry initiatives stabilize soils, maintain vegetative cover, and enhance livelihood resilience, offering alternative income sources such as fruit production or timber from fast-growing tree species. Government and NGO-led programs should incentivize adoption through subsidies, technical support, and access to markets for agroforestry products.

- Incorporate Extensive Field-Based Ground Truthing: Although the classification was validated using manually digitized points derived from high-resolution imagery, the study lacked independent field-based ground truthing. Future vegetation monitoring programs should incorporate extensive ground surveys, including GPS-referenced land cover classification, vegetation plots, and canopy structure measurements. Ground truth data would significantly improve classification accuracy, help detect subtle ecological changes, and allow calibration of remote sensing algorithms. Partnerships with local universities, forestry departments, and community organizations could facilitate cost-effective field campaigns. Establishing permanent monitoring plots in representative ecological zones would also enable long-term tracking of vegetation changes and carbon stock dynamics.

- Utilize Multi-Temporal and Multi-Sensor Remote Sensing Data: To capture more nuanced vegetation dynamics, future studies should incorporate multi-temporal remote sensing approaches, analyzing seasonal and annual vegetation trends rather than two discrete time points. Additionally, integrating data from multiple sensors would enhance monitoring capacity. For instance, Sentinel-1 SAR (Synthetic Aperture Radar) data can penetrate cloud cover and offer information on vegetation structure and moisture conditions. Landsat time series provides a longer historical context. High-resolution imagery from Planet Scope or commercial providers can improve the detection of small-scale land cover changes. Combining optical and radar datasets would provide a more comprehensive understanding of vegetation health and structural characteristics.

6.5 Future Research Directions

Future research should deepen the understanding of how socio-economic factors — including population growth, rural poverty, market demands, and land tenure systems — influence vegetation dynamics within Miombo woodlands. Integrating remote sensing analysis with household surveys, socio-economic datasets, and participatory research methods would yield a more holistic understanding of the drivers of degradation and recovery.

Climatic variability, including shifts in rainfall patterns, temperature extremes, and drought frequency, significantly influences vegetation conditions. Future studies should analyze the relationships between climate variables and vegetation trends using integrated climate and remote sensing datasets. Understanding these linkages is crucial for designing climate-resilient restoration and land management strategies. Continued long-term monitoring is essential to capture slow-onset changes, recovery trajectories, and cumulative land-use impacts. Establishing permanent monitoring sites and employing predictive modeling approaches (e.g., land-use change simulations, vegetation dynamics models) would enhance the capacity to forecast future landscape scenarios under different management and climate change pathways.

Conclusion

This study assessed spatial and temporal vegetation changes within the Miombo woodland ecosystem between 2017–2018 and 2022–2023, using Sentinel-2 imagery and a combination of threshold-based and Random Forest (RF) supervised classification approaches. By applying NDVI and EVI vegetation indices alongside spectral bands and machine learning techniques, it was possible to detect patterns of vegetation degradation, stability, and localized recovery across the landscape.

The findings revealed a largely stable landscape, interspersed with vegetation loss and gain areas. NDVI and EVI difference maps indicated that most changes were minor to moderate, with localized degradation detected primarily in the western and southwestern regions, and vegetation recovery observed along riparian corridors and isolated central zones. Threshold-based classifications offered a broad overview of these dynamics, while the RF classification captured finer fragmentation patterns and structural changes that threshold methods could not fully detect.

Accuracy assessments confirmed the strengths and limitations of the applied methods. Threshold-based classifications using manually interpreted ground truth points achieved overall accuracies of 46.1% (NDVI) and 52.2% (EVI), with moderate Kappa coefficients of 0.28 and 0.35, respectively. The Random Forest model, trained and validated using a 60/40 split, achieved 61.8% accuracy and a Kappa coefficient of 0.48, demonstrating improved performance over threshold-based methods and better alignment with the reference data. These results highlight the challenges of classifying heterogeneous woodland environments using remote sensing and emphasize the benefits of machine learning approaches.

Vegetation loss corresponded closely with known anthropogenic drivers, including agricultural expansion, fuelwood harvesting, and settlement growth. Conversely, vegetation persistence and improvement areas were associated with protected zones and riparian environments, emphasizing the resilience of Miombo woodlands where pressures are reduced or managed.

The study demonstrates that combining threshold-based and machine learning approaches provides a robust framework for monitoring vegetation dynamics in complex ecosystems. While threshold methods offer rapid assessments, Random Forest enhances mapping precision and the detection of finer-scale changes.

To further strengthen future remote sensing studies in the Miombo region, continuous monitoring using multi-temporal and multi-sensor datasets, expanded ground truth collection, and the integration of socio-economic data are recommended. Conservation strategies, sustainable land management practices, and community engagement will be vital to safeguarding the ecological and socio-economic value of the Miombo woodlands.

This research contributes valuable insights into woodland vegetation dynamics, highlights the methodological strengths and challenges of remote sensing-based classification, and provides a strong foundation for future landscape monitoring and conservation planning efforts in southern Africa's critical ecosystems.

REFERENCES

Alphan, H. (2013). Bi-Temporal Analysis of Landscape Changes in the Easternmost Mediterranean Deltas Using Binary and Classified Change Information. *Environmental Management*, *51*(3), 541–554. https://doi.org/10.1007/s00267-012-0001-9

Anchang, J. Y., Prihodko, L., Ji, W., Kumar, S. S., Ross, C. W., Yu, Q., Lind, B., Sarr, M. A., Diouf, A. A., & Hanan, N. P. (2020). Toward Operational Mapping of Woody Canopy Cover in Tropical Savannas Using Google Earth Engine. *Frontiers in Environmental Science*, *8*, 4. https://doi.org/10.3389/fenvs.2020.00004

Anyamba, A., Justice, C. O., Tucker, C. J., & Mahoney, R. (2003). Seasonal to interannual variability of vegetation and fires at SAFARI 2000 sites inferred from advanced very high resolution radiometer time series data. *Journal of Geophysical Research: Atmospheres*, *108*(D13), 2002JD002464. https://doi.org/10.1029/2002JD002464

Basalumi, L., Basalumi, L., Kilawe, C. J., & Mauya, E. W. (2018). Linking Ground Forest Inventory and NDVI in Mapping above Ground Carbon Stock in Kasane Forest Reserve, Botswana. *Open Journal of Forestry*, *08*(03), 429–438. https://doi.org/10.4236/ojf.2018.83027

Berra, E. F., Fontana, D. C., Yin, F., & Breunig, F. M. (2024). Harmonized Landsat and Sentinel-2 Data with Google Earth Engine. *Remote Sensing*, *16*(15), 2695. https://doi.org/10.3390/rs16152695

Bhattarai, S., Dons, K., & Pant, B. (2020). Assessing spatial patterns of forest degradation in dry Miombo woodland in Southern Tanzania. *Cogent Environmental Science*, *6*(1), 1801218. https://doi.org/10.1080/23311843.2020.1801218

Carvalho Júnior, O. A., Guimarães, R. F., Gillespie, A. R., Silva, N. C., & Gomes, R. A. T. (2011). A New Approach to Change Vector Analysis Using Distance and Similarity Measures. *Remote Sensing*, *3*(11), Article 11. https://doi.org/10.3390/rs3112473

Cheng, G., Huang, Y., Li, X., Lyu, S., Xu, Z., Zhao, H., Zhao, Q., & Xiang, S. (2024). Change Detection Methods for Remote Sensing in the Last Decade: A Comprehensive Review. *Remote Sensing*, *16*(13), 2355. https://doi.org/10.3390/rs16132355

Cheng, Y., Vrieling, A., Fava, F., Meroni, M., Marshall, M., & Gachoki, S. (2020). *Phenology of short vegetation cycles in a Kenyan rangeland from PlanetScope and Sentinel-2*. https://doi.org/10.1016/j.rse.2020.112004

Coppin, P., Jonckheere, I., Nackaerts, K., Muys, B., & Lambin, E. (2004). Review ArticleDigital change detection methods in ecosystem monitoring: A review. *International Journal of Remote Sensing*, *25*(9), 1565–1596. https://doi.org/10.1080/0143116031000101675

Darabi, H., Haghighi, A. T., Klöve, B., & Luoto, M. (2025). Remote sensing of vegetation trends: A review of methodological choices and sources of uncertainty. *Remote Sensing Applications: Society and Environment*, *37*, 101500. https://doi.org/10.1016/j.rsase.2025.101500

Decuyper, M., Chávez, R. O., Lohbeck, M., Lastra, J. A., Tsendbazar, N., Hackländer, J., Herold, M., & Vågen, T.-G. (2022). Continuous monitoring of forest change dynamics with satellite time series. *Remote Sensing of Environment*, *269*, 112829. https://doi.org/10.1016/j.rse.2021.112829

Delwart, S. (2015). *ESA Standard Document*. *1*.

Demol, M., Aguilar-Amuchastegui, N., Bernotaite, G., Disney, M., Duncanson, L., Elmendorp, E., Espejo, A., Furey, A., Hancock, S., Hansen, J., Horsley, H., Langa, S., Liang, M., Locke, A., Manjate, V., Mapanga, F., Omidvar, H., Parsons, A., Peneva-Reed, E., … Burt, A. (2024). Multi-scale lidar measurements suggest miombo woodlands contain substantially more carbon than thought. *Communications Earth & Environment*, *5*(1), 366. https://doi.org/10.1038/s43247-024-01448-x

Didan, K. (2015). *MYD13C2 MODIS/Aqua Vegetation Indices Monthly L3 Global 0.05Deg CMG V006* [Dataset]. NASA Land Processes Distributed Active Archive Center. https://doi.org/10.5067/MODIS/MYD13C2.006

Doxani, G., Vermote, E., Roger, J.-C., Gascon, F., Adriaensen, S., Frantz, D., Hagolle, O., Hollstein, A., Kirches, G., Li, F., Louis, J., Mangin, A., Pahlevan, N., Pflug, B., & Vanhellemont, Q. (2018). Atmospheric Correction Inter-Comparison Exercise. *Remote Sensing*, *10*(2), 352. https://doi.org/10.3390/rs10020352

Drusch, M., Del Bello, U., Carlier, S., Colin, O., Fernandez, V., Gascon, F., Hoersch, B., Isola, C., Laberinti, P., Martimort, P., Meygret, A., Spoto, F., Sy, O., Marchese, F., & Bargellini, P. (2012). Sentinel-2: ESA's Optical High-Resolution Mission for GMES Operational Services. *Remote Sensing of Environment*, *120*, 25–36. https://doi.org/10.1016/j.rse.2011.11.026

El-Hattab, M. M. (2016). Applying post classification change detection technique to monitor an Egyptian coastal zone (Abu Qir Bay). *The Egyptian Journal of Remote Sensing and Space Science*, *19*(1), 23–36. https://doi.org/10.1016/j.ejrs.2016.02.002

Frampton, W. J., Dash, J., Watmough, G., & Milton, E. J. (2013). Evaluating the capabilities of Sentinel-2 for quantitative estimation of biophysical variables in vegetation. *ISPRS Journal of Photogrammetry and Remote Sensing*, *82*, 83–92. https://doi.org/10.1016/j.isprsjprs.2013.04.007

Frost, P. (1996). *THE ECOLOGY OF MIOMBO WOODLANDS*.

Gao, Y., Solórzano, J. V., Quevedo, A., & Loya-Carrillo, J. O. (2021). How BFAST Trend and Seasonal Model Components Affect Disturbance Detection in Tropical Dry Forest and Temperate Forest. *Remote Sensing*, *13*(11), 2033. https://doi.org/10.3390/rs13112033

Generating composite images—Digital Earth Africa 2021 documentation. (2021). https://docs.digitalearthafrica.org/en/latest/sandbox/notebooks/Frequently_used_code/Generating_composites.html?utm_source=chatgpt.com

Gorelick, N., Hancher, M., Dixon, M., Ilyushchenko, S., Thau, D., & Moore, R. (2017). Google Earth Engine: Planetary-scale geospatial analysis for everyone. *Remote Sensing of Environment*, *202*, 18–27. https://doi.org/10.1016/j.rse.2017.06.031

Hagmann, R. K., Hessburg, P. F., Prichard, S. J., Povak, N. A., Brown, P. M., Fulé, P. Z., Keane, R. E., Knapp, E. E., Lydersen, J. M., Metlen, K. L., Reilly, M. J., Sánchez Meador, A. J., Stephens, S. L., Stevens, J. T., Taylor, A. H., Yocom, L. L., Battaglia, M. A., Churchill, D. J., Daniels, L. D., … Waltz, A. E. M. (2021). Evidence for widespread changes in the structure, composition, and fire regimes of western North American forests. *Ecological Applications*, *31*(8), e02431. https://doi.org/10.1002/eap.2431

Hamunyela, E., Rosca, S., Mirt, A., Engle, E., Herold, M., Gieseke, F., & Verbesselt, J. (2020). Implementation of BFASTmonitor Algorithm on Google Earth Engine to Support Large-Area and Sub-Annual Change Monitoring Using Earth Observation Data. *Remote Sensing*, *12*(18), 2953. https://doi.org/10.3390/rs12182953

Heydari, H., & Fatemi Nasrabadi, S. B. (2023). Remote sensing change detection: A comparative study of spectral distances. *Geocarto International*, *38*(1), 2248059. https://doi.org/10.1080/10106049.2023.2248059

Huete, A., Didan, K., Miura, T., Rodriguez, E. P., Gao, X., & Ferreira, L. G. (2002). Overview of the radiometric and biophysical performance of the MODIS vegetation indices. *Remote Sensing of Environment*, *83*(1–2), 195–213. https://doi.org/10.1016/S0034-4257(02)00096-2

Kalaba, F. K., Quinn, C. H., Dougill, A. J., & Vinya, R. (2013). Floristic composition, species diversity and carbon storage in charcoal and agriculture fallows and management implications in Miombo woodlands of Zambia. *Forest Ecology and Management*, *304*, 99–109. https://doi.org/10.1016/j.foreco.2013.04.024

Kamusoko, C., Gamba, J., & Murakami, H. (2014). Mapping Woodland Cover in the Miombo Ecosystem: A Comparison of Machine Learning Classifiers. *Land*, *3*(2), 524–540. https://doi.org/10.3390/land3020524

Kissanga, R., Catarino, L., Máguas, C., & Cabral, A. I. R. (2024). Dynamics of land-cover change and characterization of charcoal production and trade in southwestern Angola. *Remote Sensing Applications: Society and Environment*, *34*, 101162. https://doi.org/10.1016/j.rsase.2024.101162

Köhl, M., Baldauf, T., Plugge, D., & Krug, J. (2009). Reduced emissions from deforestation and forest degradation (REDD): A climate change mitigation strategy on a critical track. *Carbon Balance and Management*, *4*(1), 10. https://doi.org/10.1186/1750-0680-4-10

Kulindwa, K., Lein, H., Hepelwa, A., & Mshale, B. (2016). Anthropogenic Drivers of Forest Change in Miombo Ecosystems of South-eastern Tanzania: Implications for REDD+. *Tanzanian Economic Review*, *6*(1). https://doi.org/10.56279/ter.v6i1.22

Kutsch, W. L., Merbold, L., Ziegler, W., Mukelabai, M. M., Muchinda, M., Kolle, O., & Scholes, R. J. (2011). The charcoal trap: Miombo forests and the energy needs of people. *Carbon Balance and Management*, *6*(1), 5. https://doi.org/10.1186/1750-0680-6-5

Lasaponara, R., Abate, N., Fattore, C., Aromando, A., Cardettini, G., & Di Fonzo, M. (2022). On the Use of Sentinel-2 NDVI Time Series and Google Earth Engine to Detect Land-Use/Land-Cover Changes in Fire-Affected Areas. *Remote Sensing*, *14*(19), 4723. https://doi.org/10.3390/rs14194723

Li, S., Xu, L., Jing, Y., Yin, H., Li, X., & Guan, X. (2021). High-quality vegetation index product generation: A review of NDVI time series reconstruction techniques. *International Journal of Applied Earth Observation and Geoinformation*, *105*, 102640. https://doi.org/10.1016/j.jag.2021.102640

Liu, M., Zhan, Y., Li, J., Kang, Y., Sun, X., Gu, X., Wei, X., Wang, C., Li, L., Gao, H., & Yang, J. (2024). Validation of Red-Edge Vegetation Indices in Vegetation Classification in Tropical Monsoon Region—A Case Study in Wenchang, Hainan, China. *Remote Sensing*, *16*(11), 1865. https://doi.org/10.3390/rs16111865

Loew, A., Bell, W., Brocca, L., Bulgin, C. E., Burdanowitz, J., Calbet, X., Donner, R. V., Ghent, D., Gruber, A., Kaminski, T., Kinzel, J., Klepp, C., Lambert, J., Schaepman-Strub, G., Schröder, M., & Verhoelst, T. (2017). Validation practices for satellite-based Earth observation data across communities. *Reviews of Geophysics*, *55*(3), 779–817. https://doi.org/10.1002/2017RG000562

Loiola, T. M., Fantinel, R. A., Dos Santos, F. D., De Bastos, F., Schuh, M. S., Fernandes, P., Simões, B. A., & Pereira, R. S. (2023). Use of Machine Learning Algorithms in the Classification of Forest Species. *Anuário Do Instituto de Geociências*, *46*. https://doi.org/10.11137/1982-3908_2023_46_50490

López-Amoedo, A., Álvarez, X., Lorenzo, H., & Rodríguez, J. L. (2021). Multi-Temporal Sentinel-2 Data Analysis for Smallholding Forest Cut Control. *Remote Sensing*, *13*(15), 2983. https://doi.org/10.3390/rs13152983

Lu, D., Mausel, P., Brondízio, E., & Moran, E. (2004). Change detection techniques. *International Journal of Remote Sensing*, *25*(12), 2365–2401. https://doi.org/10.1080/0143116031000139863

Macarringue, L. S., Bolfe, É. L., Duverger, S. G., Sano, E. E., Caldas, M. M., Ferreira, M. C., Zullo Junior, J., & Matias, L. F. (2023). Land Use and Land Cover Classification in the Northern Region of Mozambique Based on Landsat Time Series and Machine Learning. *ISPRS International Journal of Geo-Information*, *12*(8), 342. https://doi.org/10.3390/ijgi12080342

Magalhães, T. M. (2025). What is left in miombo woodlands? Rarity and commonness of woody species, commercial timber species, and lawful harvestable diameter classes. *Heliyon*, *11*(2), e41821. https://doi.org/10.1016/j.heliyon.2025.e41821

Meneses, O. M., Ribeiro, N. S., Shirvani, Z., & Andrew, S. M. (2024). Resilience of the Miombo Woodland to Different Fire Frequencies in the LevasFlor Forest Concession, Central Mozambique. *Forests*, *16*(1), 10. https://doi.org/10.3390/f16010010

Modest, R., Maganga, S., Hassan, S., Mariki, S., & Muganda, M. (2011). Population Structure and Exploitation of Three Commercial Tree Species in Nguru ya Ndege Forest Reserve,

Morogoro – Tanzania. *Ethiopian Journal of Environmental Studies and Management*, *3*(3). https://doi.org/10.4314/ejesm.v3i3.63964

Montfort, F., Nourtier, M., Grinand, C., Maneau, S., Mercier, C., Roelens, J.-B., & Blanc, L. (2021). Regeneration capacities of woody species biodiversity and soil properties in Miombo woodland after slash-and-burn agriculture in Mozambique. *Forest Ecology and Management*, *488*, 119039. https://doi.org/10.1016/j.foreco.2021.119039

Mureva, A., Magombedze, C., Muvengwi, J., Jimu, L., & Mbiba, M. (2024). Assessing structure, spatial patterning, and size class distribution of miombo woodland species along a precipitation gradient. *South African Journal of Botany*, *171*, 173–184. https://doi.org/10.1016/j.sajb.2024.06.003

Muteya, H. K., Nghonda, D. N., Kalenda, F. M., Strammer, H., Kankumbi, F. M., Malaisse, F., Bastin, J.-F., Sikuzani, Y. U., & Bogaert, J. (2023). Mapping and Quantification of Miombo Deforestation in the Lubumbashi Charcoal Production Basin (DR Congo): Spatial Extent and Changes between 1990 and 2022. *Land*, *12*(10), 1852. https://doi.org/10.3390/land12101852

Mutowo, G. (2018). Mapping foliar N in miombo woodlands using sentinel-2 derived chlorophyll and structural indices. *Journal of Applied Remote Sensing*, *12*(04), 1. https://doi.org/10.1117/1.JRS.12.046028

NDVI, the Foundation for Remote Sensing Phenology | U.S. Geological Survey. (2018, November 29). https://www.usgs.gov/special-topics/remote-sensing-phenology/science/ndvi-foundation-remote-sensing-phenology

Nghiyalwa, H. S., Urban, M., Baade, J., Smit, I. P. J., Ramoelo, A., Mogonong, B., & Schmullius, C. (2021). Spatio-Temporal Mixed Pixel Analysis of Savanna Ecosystems: A Review. *Remote Sensing*, *13*(19), 3870. https://doi.org/10.3390/rs13193870

Nguyen, T. V., Allen, K. J., Le, N. C., Truong, C. Q., Tenzin, K., & Baker, P. J. (2023). Human-Driven Fire Regime Change in the Seasonal Tropical Forests of Central Vietnam. *Geophysical Research Letters*, *50*(13), e2022GL100687. https://doi.org/10.1029/2022GL100687

Nkya, S. E., Shirima, D. D., Masolele, R. N., Hedenas, H., & Temu, A. B. (2024a). Mapping dominant tree species of miombo woodlands in Western Tanzania using PlanetScope imagery. *Discover Applied Sciences*, *6*(10), 528. https://doi.org/10.1007/s42452-024-06248-8

Nkya, S. E., Shirima, D. D., Masolele, R. N., Hedenas, H., & Temu, A. B. (2024b). Modeling the Land Surface Phenological Responses of Dominant Miombo Tree Species to Climate Variability in Western Tanzania. *Remote Sensing*, *16*(22), 4261. https://doi.org/10.3390/rs16224261

Nogueira Lisboa, S., Grinand, C., Betbeder, J., Montfort, F., & Blanc, L. (2024). Disentangling the drivers of deforestation and forest degradation in the Miombo landscape: A case study from Mozambique. *International Journal of Applied Earth Observation and Geoinformation*, *130*, 103904. https://doi.org/10.1016/j.jag.2024.103904

N'tambwe Nghonda, D., Khoji Muteya, H., Mpanda Mukenza, M., Cabala Kaleba, S., Malaisse, F., Koy, J. K., Masengo Kalenga, W., Bogaert, J., & Useni Sikuzani, Y. (2025). Exploring the Role of Traditional Ecological Knowledge in Restoring and Managing Miombo Woodlands: A Case Study from the Lubumbashi Region, Democratic Republic of the Congo. *Forests*, *16*(3), 435. https://doi.org/10.3390/f16030435

Osazuwa-Peters, O. L., Chapman, C. A., & Zanne, A. E. (2015). Selective logging: Does the imprint remain on tree structure and composition after 45 years? *Conservation Physiology*, *3*(1), cov012. https://doi.org/10.1093/conphys/cov012

Panuju, D. R., Paull, D. J., & Griffin, A. L. (2020). Change Detection Techniques Based on Multispectral Images for Investigating Land Cover Dynamics. *Remote Sensing*, *12*(11), 1781. https://doi.org/10.3390/rs12111781

Peiman, R. (2011). Pre-classification and post-classification change-detection techniques to monitor land-cover and land-use change using multi-temporal Landsat imagery: A case study on Pisa Province in Italy. *International Journal of Remote Sensing*, *32*(15), 4365–4381. https://doi.org/10.1080/01431161.2010.486806

Phiri, D., & Morgenroth, J. (2017). Developments in Landsat Land Cover Classification Methods: A Review. *Remote Sensing*, *9*(9), 967. https://doi.org/10.3390/rs9090967

Phiri, D., Simwanda, M., Salekin, S., Nyirenda, V., Murayama, Y., & Ranagalage, M. (2020). Sentinel-2 Data for Land Cover/Use Mapping: A Review. *Remote Sensing*, *12*(14), 2291. https://doi.org/10.3390/rs12142291

Pungulanhe, L. A., S. Ribeiro, N., & M. C. Veterano, T. (2021). Frequency of Fires in the Miombo Woodland of the Gilé National Park. Province of Zambezia. *Journal of Environment and Ecology*, *12*(2), 11. https://doi.org/10.5296/jee.v12i2.19367

Qiao, K., Zhu, W., Xie, Z., Wu, S., & Li, S. (2024). New three red-edge vegetation index (VI3RE) for crop seasonal LAI prediction using Sentinel-2 data. *International Journal of Applied Earth Observation and Geoinformation*, *130*, 103894. https://doi.org/10.1016/j.jag.2024.103894

Rahimi, E., & Jung, C. (2024). Evaluating the applicability of landsat 8 data for global time series analysis. *Frontiers in Remote Sensing*, *5*, 1492534. https://doi.org/10.3389/frsen.2024.1492534

Ribeiro, N. S., Grundy, I. M., Gonçalves, F. M. P., Moura, I., Santos, M. J., Kamoto, J., Ribeiro-Barros, A. I., & Gandiwa, E. (2020). People in the Miombo Woodlands: Socio-Ecological Dynamics. In N. S. Ribeiro, Y. Katerere, P. W. Chirwa, & I. M. Grundy (Eds.), *Miombo Woodlands in a Changing Environment: Securing the Resilience and Sustainability of People and Woodlands* (pp. 55–100). Springer International Publishing. https://doi.org/10.1007/978-3-030-50104-4_3

Runge, A., & Grosse, G. (2019). Comparing Spectral Characteristics of Landsat-8 and Sentinel-2 Same-Day Data for Arctic-Boreal Regions. *Remote Sensing*, *11*(14), 1730. https://doi.org/10.3390/rs11141730

Ryan, C. M., Pritchard, R., McNicol, I., Owen, M., Fisher, J. A., & Lehmann, C. (2016). Ecosystem services from southern African woodlands and their future under global change. *Philosophical Transactions of the Royal Society B: Biological Sciences*, *371*(1703), 20150312. https://doi.org/10.1098/rstb.2015.0312

Ryan, C. M., & Williams, M. (2011). How does fire intensity and frequency affect miombo woodland tree populations and biomass? *Ecological Applications*, *21*(1), 48–60. https://doi.org/10.1890/09-1489.1

S2 Processing. (2025). https://sentiwiki.copernicus.eu/web/s2-processing

Schmitt, M., Hughes, L. H., Qiu, C., & Zhu, X. X. (2019). AGGREGATING CLOUD-FREE SENTINEL-2 IMAGES WITH GOOGLE EARTH ENGINE. *ISPRS Annals of the Photogrammetry, Remote Sensing and Spatial Information Sciences*, *IV-2/W7*, 145–152. https://doi.org/10.5194/isprs-annals-IV-2-W7-145-2019

Schneibel, A., Frantz, D., Röder, A., Stellmes, M., Fischer, K., & Hill, J. (2017). Using Annual Landsat Time Series for the Detection of Dry Forest Degradation Processes in South-Central Angola. *Remote Sensing*, *9*(9), 905. https://doi.org/10.3390/rs9090905

Scoles, S. (2022, June). These Satellites See Through the Clouds to Track Flooding. *Wired*. https://www.wired.com/story/these-satellites-see-through-the-clouds-to-track-flooding/

Smith, G. (2021, June 15). *Lessons from Zambia on promoting sustainable wood fuel management*. CIFOR-ICRAF Forests News. https://forestsnews.cifor.org/72972/lessons-from-zambia-on-promoting-sustainable-wood-fuel-management?fnl=en

Springer, K., Wang, R., & Gamon, J. (2017). Parallel Seasonal Patterns of Photosynthesis, Fluorescence, and Reflectance Indices in Boreal Trees. *Remote Sensing*, *9*(7), 691. https://doi.org/10.3390/rs9070691

Staver, A. C., Archibald, S., & Levin, S. (2011). Tree cover in sub-Saharan Africa: Rainfall and fire constrain forest and savanna as alternative stable states. *Ecology*, *92*(5), 1063–1072. https://doi.org/10.1890/10-1684.1

Staver, A. C., & Bond, W. J. (2014). Is there a 'browse trap'? Dynamics of herbivore impacts on trees and grasses in an African savanna. *Journal of Ecology*, *102*(3), 595–602. https://doi.org/10.1111/1365-2745.12230

Thornley, R., Spencer, M., Zitzer, H. R., & Parr, C. L. (2020). Woody vegetation damage by the African elephant during severe drought at Pongola Game Reserve, South Africa. *African Journal of Ecology*, *58*(4), 658–673. https://doi.org/10.1111/aje.12736

Timberlake, J., & Chidumayo, E. (2011). *MIOMBO ECOREGION VISION REPORT - Jonathan Timberlake & Emmanuel Chidumayo Occasional Publications in Biodiversity No. 20—Biofund*. https://www.readkong.com/page/miombo-ecoregion-vision-report-jonathan-timberlake-8228894

Ulsig, L., Nichol, C., Huemmrich, K., Landis, D., Middleton, E., Lyapustin, A., Mammarella, I., Levula, J., & Porcar-Castell, A. (2017). Detecting Inter-Annual Variations in the Phenology of Evergreen Conifers Using Long-Term MODIS Vegetation Index Time Series. *Remote Sensing*, *9*(1), 49. https://doi.org/10.3390/rs9010049

Useni Sikuzani, Y., Mpanda Mukenza, M., Kikuni Tchowa, J., Kabamb Kanyimb, D., Malaisse, F., & Bogaert, J. (2024). Hierarchical Analysis of Miombo Woodland Spatial Dynamics in Lualaba Province (Democratic Republic of the Congo), 1990–2024: Integrating Remote Sensing and Landscape Ecology Techniques. *Remote Sensing*, *16*(20), 3903. https://doi.org/10.3390/rs16203903

Valdivieso-Ros, C., Alonso-Sarria, F., & Gomariz-Castillo, F. (2021). Effect of Different Atmospheric Correction Algorithms on Sentinel-2 Imagery Classification Accuracy in a Semiarid Mediterranean Area. *Remote Sensing*, *13*(9), 1770. https://doi.org/10.3390/rs13091770

Van Passel, J., De Keersmaecker, W., & Somers, B. (2020). Monitoring Woody Cover Dynamics in Tropical Dry Forest Ecosystems Using Sentinel-2 Satellite Imagery. *Remote Sensing*, *12*(8), 1276. https://doi.org/10.3390/rs12081276

Vinya, R., Malhi, Y., Brown, N. D., Fisher, J. B., Brodribb, T., & Aragão, L. E. O. C. (2019). Seasonal changes in plant–water relations influence patterns of leaf display in Miombo woodlands: Evidence of water conservative strategies. *Tree Physiology*, *39*(1), 104–112. https://doi.org/10.1093/treephys/tpy062

Waldeland, A. U., Trier, Ø. D., & Salberg, A.-B. (2022). Forest mapping and monitoring in Africa using Sentinel-2 data and deep learning. *International Journal of Applied Earth Observation and Geoinformation*, *111*, 102840. https://doi.org/10.1016/j.jag.2022.102840

Walz, J. H., & Weber, K. T. (2021). *IDENTIFYING ACTIVELY GROWING VEGETATION USING NDVI THRESHOLD VALUES*. https://doi.org/10.13140/RG.2.2.18166.93769

Watts, L. M., & Laffan, S. W. (2014). Effectiveness of the BFAST algorithm for detecting vegetation response patterns in a semi-arid region. *Remote Sensing of Environment*, *154*, 234–245. https://doi.org/10.1016/j.rse.2014.08.023

Wu, X., Shen, X., Zhang, Z., Cao, F., She, G., & Cao, L. (2022). An Advanced Framework for Multi-Scale Forest Structural Parameter Estimations Based on UAS-LiDAR and Sentinel-2 Satellite Imagery in Forest Plantations of Northern China. *Remote Sensing*, *14*(13), 3023. https://doi.org/10.3390/rs14133023

Wulder, M. A., Loveland, T. R., Roy, D. P., Crawford, C. J., Masek, J. G., Woodcock, C. E., Allen, R. G., Anderson, M. C., Belward, A. S., Cohen, W. B., Dwyer, J., Erb, A., Gao, F., Griffiths, P., Helder, D., Hermosilla, T., Hipple, J. D., Hostert, P., Hughes, M. J., … Zhu, Z. (2019). Current status of Landsat program, science, and applications. *Remote Sensing of Environment*, *225*, 127–147. https://doi.org/10.1016/j.rse.2019.02.015

Yue, Y., Wang, L., Brandt, M., Zhang, X., & Wang, K. (2024). A Social-Ecological Framework to Enhance Sustainable Reforestation Under Geological Constraints. *Earth's Future*, *12*(5), e2023EF004335. https://doi.org/10.1029/2023EF004335

Zhang, X., Friedl, M. A., Schaaf, C. B., Strahler, A. H., Hodges, J. C. F., Gao, F., Reed, B. C., & Huete, A. (2003). Monitoring vegetation phenology using MODIS. *Remote Sensing of Environment*, *84*(3), 471–475. https://doi.org/10.1016/S0034-4257(02)00135-9

Zhang, Y., Wang, L., Zhou, Q., Tang, F., Zhang, B., Huang, N., & Nath, B. (2022). Continuous Change Detection and Classification—Spectral Trajectory Breakpoint Recognition for Forest Monitoring. *Land*, *11*(4), 504. https://doi.org/10.3390/land11040504

Zhu, Z., Fu, Y., Woodcock, C. E., Olofsson, P., Vogelmann, J. E., Holden, C., Wang, M., Dai, S., & Yu, Y. (2016). Including land cover change in analysis of greenness trends using all available Landsat 5, 7, and 8 images: A case study from Guangzhou, China (2000–2014). *Remote Sensing of Environment*, *185*, 243–257. https://doi.org/10.1016/j.rse.2016.03.036

Zimba, H. M., Coenders-Gerrits, M., Banda, K. E., Hulsman, P., Van De Giesen, N., Nyambe, I. A., & Savenije, H. H. G. (2024). On the importance of plant phenology in the evaporative process of a semi-arid woodland: Could it be why satellite-based evaporation estimates in the miombo differ? *Hydrology and Earth System Sciences*, *28*(15), 3633–3663. https://doi.org/10.5194/hess-28-3633-2024

APPENDIX

Appendix A: Google Earth Engine (GEE) Code

```
// Miombo Woodland Change Detection with Mixed Sentinel-2 Collections
// Uses S2 (L1C) for 2017-2018 and S2_SR (L2A) for 2022-2023

// 1. Define study area
var studyArea = ee.Geometry.Rectangle([31.5, -13.5, 32.5, -12.5]);
Map.centerObject(studyArea, 9);
Map.addLayer(studyArea, {color: 'red'}, 'Study Area');

// 2. Define time periods
var period1718 = { start: '2017-05-01', end: '2018-04-30' };
var period2223 = { start: '2022-05-01', end: '2023-04-30' };

// 3. Function to get composite from S2 (L1C) collection (for 2017-2018)
function getL1CComposite(period) {
  var collection = ee.ImageCollection("COPERNICUS/S2")
    .filterBounds(studyArea)
    .filterDate(period.start, period.end)
    .filter(ee.Filter.lt('CLOUDY_PIXEL_PERCENTAGE', 50))
    .map(function(image) {
      // Cloud masking
      var qa = image.select('QA60');
      var mask = qa.bitwiseAnd(1 << 10).eq(0).and(qa.bitwiseAnd(1 << 11).eq(0));

      // Apply reflectance scaling (old baseline)
      return image.updateMask(mask)
        .select(['B2', 'B3', 'B4', 'B8'])
        .divide(10000)  // Scale to reflectance
        .copyProperties(image, ['system:time_start']);
    });

  return collection.median().clip(studyArea);
}

// 4. Function to get composite from S2_SR (L2A) collection (for 2022-2023)
function getL2AComposite(period) {
  var collection = ee.ImageCollection("COPERNICUS/S2_SR")
    .filterBounds(studyArea)
```

```
    .filterDate(period.start, period.end)
    .filter(ee.Filter.lt('CLOUDY_PIXEL_PERCENTAGE', 50))
    .map(function(image) {
      // Cloud masking
      var scl = image.select('SCL');
      var mask = scl.neq(3)  // Cloud shadow
                 .and(scl.neq(8))  // Cloud medium probability
                 .and(scl.neq(9))  // Cloud high probability
                 .and(scl.neq(10)); // Cirrus

      // Apply reflectance scaling (new baseline)
      return image.updateMask(mask)
        .select(['B2', 'B3', 'B4', 'B8'])
        .add(-1000)  // Apply BOA_ADD_OFFSET
        .divide(10000)  // Apply QUANTIFICATION_VALUE
        .copyProperties(image, ['system:time_start']);
    });

  return collection.median().clip(studyArea);
}

// 5. Get composites for both time periods
var composite1718 = getL1CComposite(period1718);
var composite2223 = getL2AComposite(period2223);

// 6. Calculate indices
function addIndices(image) {
  var ndvi = image.normalizedDifference(['B8', 'B4']).rename('NDVI');
  var evi = image.expression(
    '2.5 * ((NIR - RED) / (NIR + 6 * RED - 7.5 * BLUE + 1))', {
      'NIR': image.select('B8'),
      'RED': image.select('B4'),
      'BLUE': image.select('B2')
    }).rename('EVI');
  return image.addBands(ndvi).addBands(evi);
}

var composite1718WithIndices = addIndices(composite1718);
var composite2223WithIndices = addIndices(composite2223);
```

```
var ndvi1718 = composite1718WithIndices.select('NDVI');
var ndvi2223 = composite2223WithIndices.select('NDVI');
var evi1718 = composite1718WithIndices.select('EVI');
var evi2223 = composite2223WithIndices.select('EVI');

// 7. Print statistics to verify expected ranges
var ndvi1718Stats = ndvi1718.reduceRegion({
  reducer: ee.Reducer.minMax(),
  geometry: studyArea,
  scale: 30,
  maxPixels: 1e9
});

var ndvi2223Stats = ndvi2223.reduceRegion({
  reducer: ee.Reducer.minMax(),
  geometry: studyArea,
  scale: 30,
  maxPixels: 1e9
});

var evi1718Stats = evi1718.reduceRegion({
  reducer: ee.Reducer.minMax(),
  geometry: studyArea,
  scale: 30,
  maxPixels: 1e9
});

var evi2223Stats = evi2223.reduceRegion({
  reducer: ee.Reducer.minMax(),
  geometry: studyArea,
  scale: 30,
  maxPixels: 1e9
});

print('NDVI 2017-2018 range:', ndvi1718Stats);
print('NDVI 2022-2023 range:', ndvi2223Stats);
print('EVI 2017-2018 range:', evi1718Stats);
print('EVI 2022-2023 range:', evi2223Stats);

// 8. Vegetation Classification
```

```
function classifyNDVI(ndvi) {
  return ndvi.expression(
    'NDVI < 0.2 ? 1 : NDVI < 0.4 ? 2 : NDVI < 0.6 ? 3 : 4',
    {'NDVI': ndvi}).rename('Veg_Class');
}

// EVI-based classification
function classifyEVI(evi) {
  return evi.expression(
    'EVI < 0.15 ? 1 : EVI < 0.35 ? 2 : EVI < 0.5 ? 3 : 4',
    {'EVI': evi}
  ).rename('EVI_Veg_Class');
}
var vegClass1718 = classifyNDVI(ndvi1718);
var vegClass2223 = classifyNDVI(ndvi2223);
var eviClass1718 = classifyEVI(evi1718);
var eviClass2223 = classifyEVI(evi2223);

// 9. Add layers to map
// Visualization parameters
var ndviVis = {
  min: 0,
  max: 0.8,
  palette: ['#FFFFFF', '#FFFCB8', '#F9F99D', '#B8E55E', '#5EB828', '#086A07']
};

var eviVis = {
  min: 0,
  max: 2.5,
  palette: ['#FFFFFF', '#FFFCB8', '#F9F99D', '#B8E55E', '#5EB828', '#086A07']
};

var vegClassVis = {
  min: 1,
  max: 4,
  palette: ['#d73027', '#fee08b', '#a6d96a', '#1a9850']
};

// Add main layers
Map.addLayer(ndvi1718, ndviVis, 'NDVI 2017-2018');
```

```
Map.addLayer(ndvi2223, ndviVis, 'NDVI 2022-2023');
Map.addLayer(evi1718, eviVis, 'EVI 2017-2018');
Map.addLayer(evi2223, eviVis, 'EVI 2022-2023');
Map.addLayer(vegClass1718, vegClassVis, 'NDVI Veg Class 2017-2018', false);
Map.addLayer(vegClass2223, vegClassVis, 'NDVI Veg Class 2022-2023', false);
Map.addLayer(eviClass1718, vegClassVis, 'EVI Veg Class 2017-2018', false);
Map.addLayer(eviClass2223, vegClassVis, 'EVI Veg Class 2022-2023', false);

// RGB composites for reference
var rgbVis = {
  bands: ['B4', 'B3', 'B2'],
  min: 0,
  max: 0.3
};

Map.addLayer(composite1718, rgbVis, 'RGB 2017-2018', false);
Map.addLayer(composite2223, rgbVis, 'RGB 2022-2023', false);

// 10. Export corrected images
// Export NDVI
Export.image.toDrive({
  image: ndvi1718,
  description: 'Mixed_Corrected_NDVI_2017_2018',
  folder: 'GEE_Exports_Corrected',
  scale: 10,
  region: studyArea,
  maxPixels: 1e9
});

Export.image.toDrive({
  image: ndvi2223,
  description: 'Mixed_Corrected_NDVI_2022_2023',
  folder: 'GEE_Exports_Corrected',
  scale: 10,
  region: studyArea,
  maxPixels: 1e9
});

// Export EVI
Export.image.toDrive({
```

```
  image: evi1718,
  description: 'Mixed_Corrected_EVI_2017_2018',
  folder: 'GEE_Exports_Corrected',
  scale: 10,
  region: studyArea,
  maxPixels: 1e9
});

Export.image.toDrive({
  image: evi2223,
  description: 'Mixed_Corrected_EVI_2022_2023',
  folder: 'GEE_Exports_Corrected',
  scale: 10,
  region: studyArea,
  maxPixels: 1e9
});

// Export classification
Export.image.toDrive({
  image: vegClass1718,
  description: 'Mixed_Corrected_NDVI_VegClass_2017_2018',
  folder: 'GEE_Exports_Corrected',
  scale: 10,
  region: studyArea,
  maxPixels: 1e9
});

Export.image.toDrive({
  image: vegClass2223,
  description: 'Mixed_Corrected_NDVI_VegClass_2022_2023',
  folder: 'GEE_Exports_Corrected',
  scale: 10,
  region: studyArea,
  maxPixels: 1e9
});

Export.image.toDrive({
  image: eviClass1718,
  description: 'Mixed_Corrected_EVI_VegClass_2017_2018',
  folder: 'GEE_Exports_Corrected',
```

```
  scale: 10,
  region: studyArea,
  maxPixels: 1e9
});

Export.image.toDrive({
  image: eviClass2223,
  description: 'Mixed_Corrected_EVI_VegClass_2022_2023',
  folder: 'GEE_Exports_Corrected',
  scale: 10,
  region: studyArea,
  maxPixels: 1e9
});

// Script to check Sentinel-2 processing baseline information
// This helps determine which scaling approach to use for reflectance

// Define study area (change coordinates as needed)
var studyArea = ee.Geometry.Rectangle([31.5, -13.5, 32.5, -12.5]);
Map.centerObject(studyArea, 9);
Map.addLayer(studyArea, {color: 'red'}, 'Study Area');

// Define time periods to check
var periods = [
  {name: '2017', start: '2017-05-01', end: '2017-05-31'},
  {name: '2018', start: '2018-05-01', end: '2018-05-31'},
  {name: '2019', start: '2019-05-01', end: '2019-05-31'},
  {name: '2020', start: '2020-05-01', end: '2020-05-31'},
  {name: '2021', start: '2021-05-01', end: '2021-05-31'},
  {name: '2022', start: '2022-05-01', end: '2022-05-31'},
  {name: '2023', start: '2023-05-01', end: '2023-05-31'}
];

// Check L1C (TOA) collection
print('CHECKING SENTINEL-2 L1C COLLECTION (COPERNICUS/S2)');
periods.forEach(function(period) {
  var image = ee.ImageCollection('COPERNICUS/S2')
    .filterBounds(studyArea)
    .filterDate(period.start, period.end)
    .first();
```

```
  if (image) {
    print(period.name + ' L1C first image date:',
      ee.Date(image.get('system:time_start')).format('YYYY-MM-dd'));

    // Try to get processing baseline directly
    var baseline = image.get('PROCESSING_BASELINE');
    print(period.name + ' L1C processing baseline:', baseline);

    // Print some key metadata to inspect
    var metadata = {
      'Mission ID': image.get('MISSION_ID'),
      'Product ID': image.get('PRODUCT_ID')
    };
    print(period.name + ' L1C metadata:', metadata);
  } else {
    print(period.name + ' L1C: No images available');
  }
});

// Check L2A (SR) collection
print('CHECKING SENTINEL-2 L2A COLLECTION (COPERNICUS/S2_SR)');
periods.forEach(function(period) {
  var image = ee.ImageCollection('COPERNICUS/S2_SR')
    .filterBounds(studyArea)
    .filterDate(period.start, period.end)
    .first();

  if (image) {
    print(period.name + ' L2A first image date:',
      ee.Date(image.get('system:time_start')).format('YYYY-MM-dd'));

    // Try to get processing baseline directly
    var baseline = image.get('PROCESSING_BASELINE');
    print(period.name + ' L2A processing baseline:', baseline);

    // Print some key metadata to inspect
    var metadata = {
      'Mission ID': image.get('MISSION_ID'),
      'Product ID': image.get('PRODUCT_ID')
```

```
    };
    print(period.name + ' L2A metadata:', metadata);

    // Sample a point to check raw values
    if (period.name === '2017' || period.name === '2022') {
      var samplePoint = ee.Geometry.Point([31.75, -13.0]);
      var sample = image.select(['B2', 'B3', 'B4', 'B8']).sample(samplePoint, 30).first();
      print(period.name + ' L2A sample pixel values:', sample);
    }
  } else {
    print(period.name + ' L2A: No images available');
  }
});



// NDVI Change Map: Encode transitions
var ndviChangeMap = vegClass1718.multiply(10).add(vegClass2223).rename('NDVI_Change_Map');

// Visualization settings
var ndviChangeMapVis = {
  min: 11,
  max: 44,
  palette: [
    '#969696', '#fdd0a2', '#a1d99b', '#31a354',  // Example colors
    '#fc9272', '#fb6a4a', '#ef3b2c', '#cb181d',
    '#a50f15', '#a6bddb', '#74a9cf', '#3690c0',
    '#0570b0', '#045a8d'
  ]
};

// Add NDVI Change Map to map
Map.addLayer(ndviChangeMap, ndviChangeMapVis, 'NDVI Change Map');

// NDVI Change Direction:
// 1 = No change
// 2 = Degradation (class decrease)
// 3 = Improvement (class increase)
var ndviChangeDirection = ee.Image(0)
  .where(vegClass1718.eq(vegClass2223), 1) // No change
```

```
  .where(vegClass1718.gt(vegClass2223), 2) // Decrease
  .where(vegClass1718.lt(vegClass2223), 3) // Increase
  .rename('NDVI_Change_Direction');

// Visualization settings
var ndviChangeDirVis = {
  min: 1,
  max: 3,
  palette: ['#969696', '#d73027', '#1a9850']  // Grey = No change, Red = Loss, Green = Gain
};

// Add NDVI Change Direction Map
Map.addLayer(ndviChangeDirection, ndviChangeDirVis, 'NDVI Change Direction');

// EVI Change Map
var eviChangeMap = eviClass1718.multiply(10).add(eviClass2223).rename('EVI_Change_Map');

// Visualization settings
var eviChangeMapVis = {
  min: 11,
  max: 44,
  palette: [
    '#a50026', '#d73027', '#f46d43', '#fdae61',
    '#fee08b', '#d9ef8b', '#a6d96a', '#66bd63',
    '#1a9850', '#66c2a5', '#3288bd', '#5e4fa2'
  ]
};

// Add EVI Change Map to map
Map.addLayer(eviChangeMap, eviChangeMapVis, 'EVI Change Map');

// EVI Change Direction
var eviChangeDirection = ee.Image(0)
  .where(eviClass1718.eq(eviClass2223), 1) // No change
  .where(eviClass1718.gt(eviClass2223), 2) // Decrease
  .where(eviClass1718.lt(eviClass2223), 3) // Increase
  .rename('EVI_Change_Direction');

// Visualization settings
var eviChangeDirVis = {
```

```
  min: 1,
  max: 3,
  palette: ['#969696', '#d73027', '#1a9850']
};

// Add EVI Change Direction Map
Map.addLayer(eviChangeDirection, eviChangeDirVis, 'EVI Change Direction');



// Export NDVI Change Map
Export.image.toDrive({
  image: ndviChangeMap,
  description: 'NDVI_Change_Map_2017_2023',
  folder: 'GEE_Exports_Corrected',
  fileNamePrefix: 'NDVI_Change_Map_2017_2023',
  scale: 10,
  region: studyArea,
  maxPixels: 1e9
});

// Export NDVI Change Direction Map
Export.image.toDrive({
  image: ndviChangeDirection,
  description: 'NDVI_Change_Direction_2017_2023',
  folder: 'GEE_Exports_Corrected',
  fileNamePrefix: 'NDVI_Change_Direction_2017_2023',
  scale: 10,
  region: studyArea,
  maxPixels: 1e9
});

// Export EVI Change Map
Export.image.toDrive({
  image: eviChangeMap,
  description: 'EVI_Change_Map_2017_2023',
  folder: 'GEE_Exports_Corrected',
  fileNamePrefix: 'EVI_Change_Map_2017_2023',
  scale: 10,
  region: studyArea,
  maxPixels: 1e9
```

```
});

// Export EVI Change Direction Map
Export.image.toDrive({
  image: eviChangeDirection,
  description: 'EVI_Change_Direction_2017_2023',
  folder: 'GEE_Exports_Corrected',
  fileNamePrefix: 'EVI_Change_Direction_2017_2023',
  scale: 10,
  region: studyArea,
  maxPixels: 1e9
});




// NDVI Difference: 2022-2023 minus 2017-2018
var ndviDiff = ndvi2223.subtract(ndvi1718).rename('NDVI_Difference');

// Visualization settings
var ndviDiffVis = {
  min: -0.5,
  max: 0.5,
  palette: [
    '#d73027', // Strong decrease (red)
    '#f46d43',
    '#fdae61',
    '#fee08b',
    '#ffffbf', // No change (yellow)
    '#d9ef8b',
    '#a6d96a',
    '#66bd63',
    '#1a9850'  // Strong increase (green)
  ]
};

// Add NDVI Difference map
Map.addLayer(ndviDiff, ndviDiffVis, 'NDVI Difference (2022-2023 minus 2017-2018)');
```

```
// EVI Difference: 2022-2023 minus 2017-2018
var eviDiff = evi2223.subtract(evi1718).rename('EVI_Difference');

// Visualization settings
var eviDiffVis = {
  min: -1,
  max: 1,
  palette: [
    '#d73027', // Strong decrease (red)
    '#f46d43',
    '#fdae61',
    '#fee08b',
    '#ffffbf', // No change (yellow)
    '#d9ef8b',
    '#a6d96a',
    '#66bd63',
    '#1a9850'  // Strong increase (green)
  ]
};

// Add EVI Difference map
Map.addLayer(eviDiff, eviDiffVis, 'EVI Difference (2022-2023 minus 2017-2018)');

// Export NDVI Difference Map
Export.image.toDrive({
  image: ndviDiff,
  description: 'NDVI_Difference_Map_2017_2023',
  folder: 'GEE_Exports_Corrected',
  fileNamePrefix: 'NDVI_Difference_Map_2017_2023',
  scale: 10,
  region: studyArea,
  maxPixels: 1e9
});

// Export EVI Difference Map
Export.image.toDrive({
  image: eviDiff,
  description: 'EVI_Difference_Map_2017_2023',
  folder: 'GEE_Exports_Corrected',
```

```
  fileNamePrefix: 'EVI_Difference_Map_2017_2023',
  scale: 10,
  region: studyArea,
  maxPixels: 1e9
});

// Create a histogram chart for NDVI Difference
var ndviDiffChart = ui.Chart.image.histogram({
  image: ndviDiff,
  region: studyArea,
  scale: 30,
  maxPixels: 1e9
})
.setOptions({
  title: 'NDVI Difference Histogram (2017–2023)',
  hAxis: {title: 'NDVI Difference Value'},
  vAxis: {title: 'Pixel Count'},
  series: [{color: 'green'}]
});

print(ndviDiffChart);

// Create a histogram chart for EVI Difference
var eviDiffChart = ui.Chart.image.histogram({
  image: eviDiff,
  region: studyArea,
  scale: 30,
  maxPixels: 1e9
})
.setOptions({
  title: 'EVI Difference Histogram (2017–2023)',
  hAxis: {title: 'EVI Difference Value'},
  vAxis: {title: 'Pixel Count'},
  series: [{color: 'blue'}]
});

print(eviDiffChart);

// NDVI Difference Statistics
var ndviDiffStats = ndviDiff.reduceRegion({
```

```
  reducer: ee.Reducer.minMax(),
  geometry: studyArea,
  scale: 10,
  maxPixels: 1e9
});

print('NDVI Difference Min/Max:', ndviDiffStats);

// EVI Difference Statistics
var eviDiffStats = eviDiff.reduceRegion({
  reducer: ee.Reducer.minMax(),
  geometry: studyArea,
  scale: 10,
  maxPixels: 1e9
});

print('EVI Difference Min/Max:', eviDiffStats);



// 1. Load the cleaned CSV asset and rename 'class' to 'Class'
var groundTruth = ee.FeatureCollection('projects/ee-
jayamponsem/assets/Merged_Stratified_Samples_EVI_NDVI');

groundTruth = groundTruth.map(function(f) {
  return f.set('Class', f.get('class'));
});

// 2. Filter valid vegetation classes (1–4)
var correctedGroundTruth = groundTruth.filter(ee.Filter.inList('Class', [1, 2, 3, 4]));
print('Corrected Ground Truth Points:', correctedGroundTruth);
print('Number of ground truth points:', correctedGroundTruth.size());

// 3. NDVI Validation Sampling
var ndviValidation = vegClass1718.sampleRegions({
  collection: correctedGroundTruth,
  properties: ['Class'],
  scale: 10
});
print('NDVI validation sample size:', ndviValidation.size());
```

```
var ndviMatrix = ndviValidation.errorMatrix('Class', 'Veg_Class');
print('NDVI Ground Truth Confusion Matrix:', ndviMatrix);
print('NDVI Accuracy:', ndviMatrix.accuracy());
print('NDVI Kappa:', ndviMatrix.kappa());

// 4. EVI Validation Sampling
var eviValidation = eviClass1718.sampleRegions({
  collection: correctedGroundTruth,
  properties: ['Class'],
  scale: 10
});
print('EVI validation sample size:', eviValidation.size());

var eviMatrix = eviValidation.errorMatrix('Class', 'EVI_Veg_Class');
print('EVI Ground Truth Confusion Matrix:', eviMatrix);
print('EVI Accuracy:', eviMatrix.accuracy());
print('EVI Kappa:', eviMatrix.kappa());

// Add a random column to allow splitting
var withRandom = correctedGroundTruth.randomColumn('rand');

// 60% Training, 40% Validation
var trainingPoints = withRandom.filter(ee.Filter.lt('rand', 0.6));
var validationPoints = withRandom.filter(ee.Filter.gte('rand', 0.6));

print('Training sample count:', trainingPoints.size());
print('Validation sample count:', validationPoints.size());

// --- Train Random Forest ---
var inputBands = ['B2', 'B3', 'B4', 'B8'];
var rfTraining = composite1718.select(inputBands).sampleRegions({
  collection: trainingPoints,
  properties: ['Class'],
  scale: 10
});
print('RF training sample size:', rfTraining.size());

var rfClassifier = ee.Classifier.smileRandomForest(50).train({
  features: rfTraining,
```

```
  classProperty: 'Class',
  inputProperties: inputBands
});

// --- Classify ---
var rfClassified = composite1718.select(inputBands).classify(rfClassifier);

// --- Validate using the 20% hold-out set ---
var rfValidation = rfClassified.sampleRegions({
  collection: validationPoints,
  properties: ['Class'],
  scale: 10
});
print('RF validation sample size:', rfValidation.size());

var rfMatrix = rfValidation.errorMatrix('Class', 'classification');
print('RF Confusion Matrix (60/40 split):', rfMatrix);
print('RF Accuracy (60/40):', rfMatrix.accuracy());
print('RF Kappa (60/40):', rfMatrix.kappa());
```

Source: Author's work

Appendix B: Ground Truth Validation Points (Google Earth Pro)

class	longitude	latitude
1	32.19575453	-13.01663338
1	31.95383822	-13.35152532
1	32.14257427	-12.64239524
1	31.91790561	-12.98231774
1	31.92140904	-12.86409945
1	31.91997174	-12.88422171
1	31.84819635	-12.62146449
1	31.85466422	-13.14949421
1	32.11257053	-13.3890749
1	31.76025128	-13.11463958
1	32.39365339	-12.878203
1	32.25504334	-12.97611936
1	32.38251428	-12.72486058
1	32.11481632	-13.41279042
1	31.50072799	-13.00468579
1	31.9617434	-12.6474258
1	32.37362096	-12.68407706
1	32.05031729	-12.50360552
1	32.05067661	-13.29223651
1	31.95707216	-13.28010926
1	32.09316692	-13.37694764
1	32.21434966	-12.53854999
1	31.86786945	-13.28343302
1	31.92428365	-12.77435775
1	32.49354605	-12.64239524
2	31.59253582	-13.39796822
2	31.50405176	-12.81343447
2	31.74444093	-13.45402309
2	31.63403798	-13.16629271
2	31.82960122	-12.92725101

2	32.26770958	-12.65685811
2	31.73545778	-12.93515619
2	32.47351362	-12.68569403
2	32.11742144	-13.23851726
2	32.35260038	-12.86975883
2	31.80283142	-13.06828651
2	31.50198564	-13.16045366
2	31.92338534	-12.53091431
2	32.01348636	-12.82457357
2	31.67266554	-13.34038621
2	32.18003401	-12.81693789
2	31.75683768	-13.25127333
2	31.55193197	-12.8998524
2	31.59002053	-12.62999848
2	31.96102475	-13.08939692
2	32.3945517	-12.54735348
2	31.71255074	-13.20231515
2	32.33912565	-13.10898019
2	32.421052	-12.84613314
2	31.88862053	-12.71291299
3	31.69099117	-12.56181635
3	31.5884934	-12.56217568
3	31.82834358	-12.72117749
3	32.43964713	-12.57574024
3	32.04843082	-13.39626142
3	31.60870549	-13.14572129
3	31.62990573	-12.50028176
3	31.65667553	-12.8830539
3	31.55166247	-12.80777508
3	32.48240694	-12.77426792
3	31.57061692	-12.88538952
3	32.43308943	-13.2614243
3	31.60196813	-12.56666726

3	31.54088269	-12.8830539
3	31.58436115	-12.61248134
3	31.59855453	-12.97028031
3	31.75980212	-12.63781383
3	31.69692005	-12.74992357
3	31.58966121	-13.00172135
3	32.49812745	-12.98995342
3	31.83148768	-12.68533471
3	31.66835363	-12.6326036
3	31.666557	-13.44153651
3	31.63969737	-13.027503
3	31.72773227	-12.7252199
4	32.20725297	-13.22225775
4	32.40533149	-13.47549283
4	32.15425236	-13.31810799
4	31.65137547	-12.59792863
4	31.64957884	-13.34011672
4	31.6679943	-13.25405811
4	31.56414905	-13.4437823
4	32.43488606	-13.49920835
4	32.00603034	-13.27930077
4	31.64715339	-13.33634379
4	32.15488118	-13.31119096
4	32.43982679	-13.48375733
4	32.15982192	-13.25226148
4	31.54806921	-13.42743296
4	32.10861795	-13.44369247
4	31.7343798	-13.17347923
4	31.5238147	-12.53307027
4	31.99920315	-12.85511629
4	32.03926801	-12.78253242
4	32.4344369	-13.49857953
4	31.94781951	-13.43884157

4	31.6483212	-13.33589463
4	31.99938281	-12.85502646
4	32.40640946	-13.47136058
4	32.1888375	-13.23707995
1	31.59253582	-13.39796822
1	32.19575453	-13.01663338
1	31.82960122	-12.92725101
1	31.80283142	-13.06828651
1	31.50198564	-13.16045366
1	32.01348636	-12.82457357
1	31.95383822	-13.35152532
1	32.18003401	-12.81693789
1	31.75683768	-13.25127333
1	31.96102475	-13.08939692
1	32.3945517	-12.54735348
1	31.71255074	-13.20231515
1	32.33912565	-13.10898019
1	31.88862053	-12.71291299
1	32.14257427	-12.64239524
1	31.765731	-13.22998326
1	32.1671881	-13.01887917
1	31.99552005	-12.79870209
1	32.2834301	-12.86544692
1	32.16332535	-13.37685781
1	31.8870934	-12.57520125
1	31.91790561	-12.98231774
1	31.57079659	-13.20060835
1	32.00315573	-12.62927983
1	32.22566843	-13.47432502
2	31.50405176	-12.81343447
2	31.74444093	-13.45402309
2	31.63403798	-13.16629271
2	32.26770958	-12.65685811

2	31.73545778	-12.93515619
2	32.47351362	-12.68569403
2	32.11742144	-13.23851726
2	32.35260038	-12.86975883
2	31.92338534	-12.53091431
2	31.69099117	-12.56181635
2	31.67266554	-13.34038621
2	31.5884934	-12.56217568
2	31.82834358	-12.72117749
2	31.55193197	-12.8998524
2	31.59002053	-12.62999848
2	32.421052	-12.84613314
2	32.43964713	-12.57574024
2	31.59693756	-12.92581371
2	32.321878	-12.82017183
2	32.00243708	-13.23564265
2	32.04843082	-13.39626142
2	32.03962733	-13.09586479
2	32.28378943	-12.99399584
2	31.60870549	-13.14572129
2	32.21210387	-13.11688537
3	32.20725297	-13.22225775
3	32.40533149	-13.47549283
3	32.15425236	-13.31810799
3	31.65137547	-12.59792863
3	31.64957884	-13.34011672
3	32.43488606	-13.49920835
3	31.64715339	-13.33634379
3	32.15488118	-13.31119096
3	32.43982679	-13.48375733
3	32.10861795	-13.44369247
3	31.99920315	-12.85511629
3	32.4344369	-13.49857953

3	31.94781951	-13.43884157
3	31.6483212	-13.33589463
3	32.40640946	-13.47136058
3	32.1888375	-13.23707995
3	31.72090507	-13.1548841
3	32.25998407	-13.46929445
3	32.16341518	-13.33032508
3	32.40236705	-12.83768898
3	32.15631849	-13.25423778
3	31.55831	-13.42788212
3	31.94144147	-13.34496762
3	32.17410513	-13.25540559
3	31.93614141	-12.66485312
4	31.68535658	-12.89491195
4	31.68535658	-12.89491195
4	31.68526692	-12.89471068
4	31.68520839	-12.89464548
4	31.68532213	-12.89467358

Source: Author's own work

Appendix C: NDVI,EVI Ground Truth Points and Validation Summary from GEE

```
Number of ground truth points:
180
```
JSON

```
NDVI validation sample size:
180
```
JSON

```
EVI validation sample size:
180
```
JSON

Source: Google Earth Engine

Appendix D: Random Forest Training and Validation Sample Sizes from GEE

```
RF training sample size:
112
```
JSON

```
RF validation sample size:
68
```
JSON

Source: Google Earth Engine

Appendix E: NDVI Confusion Matrix Output and Class Histogram from GEE

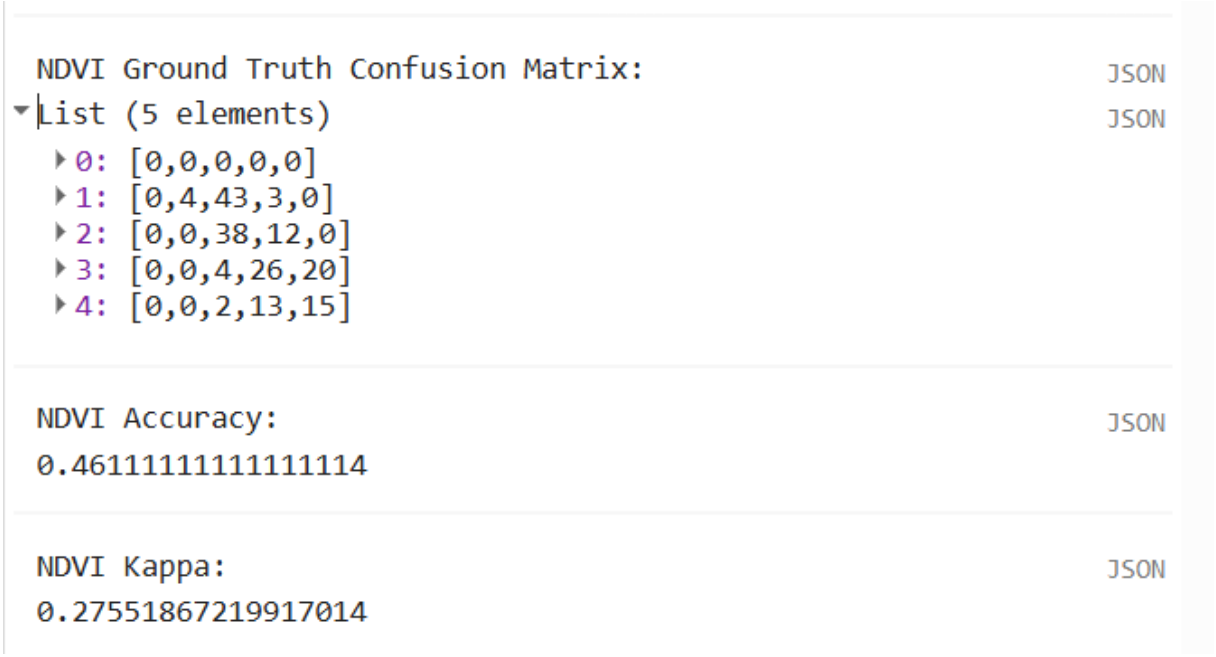

Source: Google Earth Engine

Appendix F: EVI Confusion Matrix Output and Class Histogram from GEE

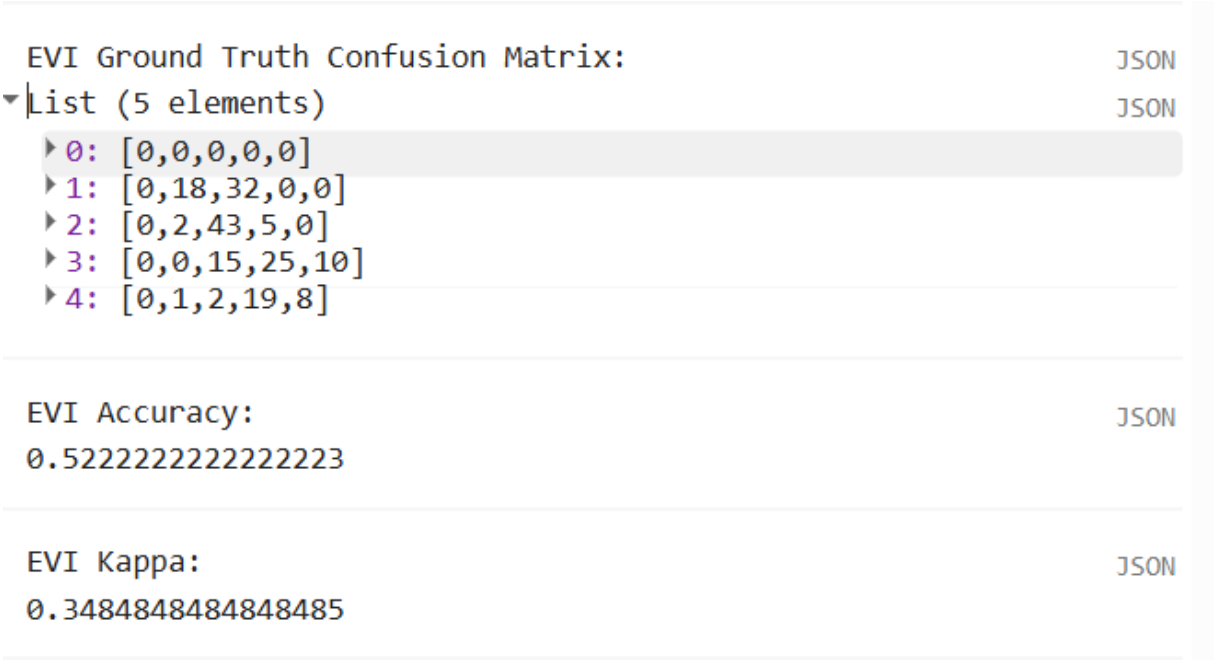

Source: Google Earth Engine

Appendix G: Random Forest Condusion Matrix Output and Class Histogram from GEE

Source: Google Earth Engine